AWARD NUMBER: W81XWH- 14-1-0192

TITLE: Next-Generation Molecular Histology Using Highly Multiplexed Ion Beam Imaging (MIBI) of Breast Cancer Tissue Specimens for Enhanced Clinical Guidance

PRINCIPAL INVESTIGATOR: Alexander Borowsky

CONTRACTING ORGANIZATION: University of California, Davis
Davis, CA 95616

REPORT DATE: July 2015

TYPE OF REPORT: Annual

PREPARED FOR: U.S. Army Medical Research and Materiel Command
Fort Detrick, Maryland 21702-5012

REPORT DOCUMENTATION PAGE

Form Approved
OMB No. 0704-0188

1. REPORT DATE	2. REPORT TYPE	3. DATES COVERED
July 2015	Annual	1Jul2014 - 30Jun2015

4. TITLE AND SUBTITLE

Next-Generation Molecular Histology Using Highly Multiplexed Ion Beam Imaging (MIBI) of Breast Cancer Tissue Specimens for Enhanced Clinical Guidance

5a. CONTRACT NUMBER
W81XWH-14-1-0192

5b. GRANT NUMBER

5c. PROGRAM ELEMENT NUMBER

6. AUTHOR(S)
Alexander Borowsky

E-Mail: adborowsky@ucdavis.edu

5d. PROJECT NUMBER

5e. TASK NUMBER

5f. WORK UNIT NUMBER

7. PERFORMING ORGANIZATION NAME(S) AND ADDRESS(ES)
University of California, Davis
One Shields Ave
Davis CA 95616

8. PERFORMING ORGANIZATION REPORT NUMBER

9. SPONSORING / MONITORING AGENCY NAME(S) AND ADDRESS(ES)

U.S. Army Medical Research and Materiel Command
Fort Detrick, Maryland 21702-5012

10. SPONSOR/MONITOR'S ACRONYM(S)

11. SPONSOR/MONITOR'S REPORT NUMBER(S)

12. DISTRIBUTION / AVAILABILITY STATEMENT

Approved for public release, Distribution Unlimited

13. SUPPLEMENTARY NOTES

14. ABSTRACT **Current breast cancer diagnosis includes predictive assays to guide therapy decisions, involving a minimum of 3assays: ER, PR, and HER2. Many labs also include a marker of proliferation (Ki67), and sometimes myoepithelial (SMA), epithelial (CK8/18), and lobular markers (ECAD). Recently, a host of new multi-marker panels developed. The "Mammostrat" assay (Clarient) uses a panel of five IHC markers (P53, SLC7A5,NRDG1, HTF9C, CEACAM5). Gene-expression assays using qRT-PCR, array hybridization, and RNA sequence assays have also been developed. The OncotypeDX, for example, uses a panel of 21 genes (16 analytical, 5 controls: Ki67, STK15, Survivin, CCNB1, MYBL2, MMP11, CTSL2, HER2, GRB7, GSTM1,CD68, BAG1, ER, PGR, BCL2, SCUBE2, ACTB, GAPDH, RPLPO, GUS, TFRC) to stratify risk of recurrence, and relative benefit of adjuvant chemotherapy. This explosion in biomarkers poses both cost and logical selection challenges. In addition, these assays generally lose all spatial context information (including heterogeneity). MIBI technology provides the potential to simultaneously assay all of the relevant analytes in an intact tissue architecture, with submicron resolution and a greatly expanded dynamic range of quantitation. We propose to develop assays and analysis tools to evaluate breast cancer tissues using formal fixed and paraffin embedded tumor tissues from the clinic, and we will compare the utility of the MIBI platform assays to the current assays. Our objective is to validate MIBI as an alternative to current standard multi-gene assays. We also hypothesize that MIBI breast cancer data will improve the ability to stratify risk and predict therapy responses by taking into account the distribution and heterogeneity of molecularly defined cell populations in breast cancer.**

15. SUBJECT TERMS

Nothing listed

16. SECURITY CLASSIFICATION OF:			17. LIMITATION OF ABSTRACT	18. NUMBER OF PAGES	19a. NAME OF RESPONSIBLE PERSON
a. REPORT	b. ABSTRACT	c. THIS PAGE			USAMRMC
Unclassified	Unclassified	Unclassified	Unclassified	46	19b. TELEPHONE NUMBER *(include area code)*

Table of Contents

INTRODUCTION:

Current breast cancer diagnosis includes predictive assays to guide therapy decisions, involving a minimum of 3assays: ER, PR, and HER2. Many labs also include a marker of proliferation (Ki67), and sometimes myoepithelial (SMA), epithelial (CK8/18), and lobular markers (ECAD). Recently, a host of new multi-marker panels developed. The “Mammostrat” assay (Clarient) uses a panel of five IHC markers (P53, SLC7A5,NRDG1, HTF9C, CEACAM5). Gene-expression assays using qRT-PCR, array hybridization, and RNA sequence assays have also been developed. The OncotypeDX, for example, uses a panel of 21 genes (16 analytical, 5 controls: Ki67, STK15, Survivin, CCNB1, MYBL2, MMP11, CTSL2, HER2, GRB7, GSTM1,CD68, BAG1, ER, PGR, BCL2, SCUBE2, ACTB, GAPDH, RPLPO, GUS, TFRC) to stratify risk of recurrence, and relative benefit of adjuvant chemotherapy. This explosion in biomarkers poses both cost and logical selection challenges. In addition, these assays generally lose all spatial context information (including heterogeneity). MIBI technology provides the potential to simultaneously assay all of the relevant analytes in an intact tissue architecture, with

submicron resolution and a greatly expanded dynamic range of quantitation. We propose to develop assays and analysis tools to evaluate breast cancer tissues using formal fixed and paraffin embedded tumor tissues from the clinic, and we will compare the utility of the MIBI platform assays to the current assays. Our *objective* is to validate MIBI as an alternative to current standard multi-gene assays. We also *hypothesize* that MIBI breast cancer data will improve the ability to stratify risk and predict therapy responses by taking into account the distribution and heterogeneity of molecularly defined cell populations in breast cancer.

KEYWORDS: *Provide a brief list of keywords (limit to 20 words).*
Breast Cancer Diagnosis
Pathology
Immunophenotype
Multiplex
Morphology
RNA In Situ Hybridization
Immunohistochemistry/immunofluorescence
Predictive Biomarkers
Quantitative Image Analysis

Body/ Key Research Accomplishments/ Reportable Outcomes:

A. What was accomplished under these goals? Statement of Work Progress Update:
Elements of each of the specific aims require work performed at both UC Davis and Stanford. Briefly, the division of labor falls into the following breakdown: All tissue procurement, tissue and cell culture handling, tissue sectioning and mounting, probe labeling, tissue probe incubations and standard curve measurements (western and qRT-PCR) will be performed in the Borowsky lab at UC Davis. All nanoSIMS imaging, initial image analysis, image segmentation and data output will be performed in the Nolan lab at Stanford. Subsequent analysis and risk stratification algorithms will be done in collaboration of all groups with the informatics team lead by Dr. Levenson at UC Davis. The following is a breakdown of specific aims into individual tasks over the three years of the grant period.
Specific Aims: In order to achieve the objectives we will develop two new multi-gene panels of MIBI multiplexed *in situ* detection reagents, and compare the quantitative data to the conventional clinically derived "one at a time" and/or "grind-it-up" assays. Meanwhile, our data analysis will provide complex cell population distributions, which will be compared to clinical outcomes. We anticipate that new discoveries of specific cell populations associated with specific outcomes or tumor biologies will require larger retrospective, and eventually prospective trials, but this proposal will enable such studies to proceed rapidly and efficiently.
Please see Figure 1 Appendix I.

Aim I: One slide complete IHC analysis: Develop the multiplex panel of the following 13 mass tagged primary antibodies for simultaneous diagnosis, categorical predictive assessment and calculation of current algorithms for risk prediction: ER, PgR, HER2, Ki67, BAG1, SMA, CK8/18, ECAD, P53, SLC7A5, NRDG1,HTF9C, CEACAM5.
Ia. Complete the currently developed 10 antibody panel (see preliminary data and pending publication *revisions submitted*, Nature Medicine) with additional antibodies to complete the 13 antibody panel.
Tasks: Ia.1 (Davis) Choose, order and test by conventional DAB/secondary antibody detection the new antibodies to complete the panel. For each, control tissue sections and breast cancers (deidentified) using conventional formalin fixed and paraffin embedded tissue blocks will be used.
Completed.
Ia.2 (Davis) Optimize titers using conventional immunohistochemistry.
Completed for 10 of 13 proposed antibodies. 3 additional in progress.
Ia.3 (Davis) Prepare mass tagged primary antibodies.
Year 2 planned.
Ia.4 (Davis) Prepare tissue samples with mass tagged antibodies: single label, double label and complete panel (13 label).
Year 2-3.
Ia.5 (Stanford) nanoSIMS MIBI imaging of single, double and panel labeled samples.
Pilot work completed, test samples Year 2.
Ia.6 (Stanford) Initial image analysis of MIBI images for display of categorical and quantitative signals.
Pilot work completed, test samples begin Year 2.
Ia.7 (Stanford) Image cell segmentation and cell distributions by 13x immunophenotype and cell morphology.
Follows Aims Ia.6 and 7.

Ib. Measure standard curves for each analyte against western blots using cell lines and tumor samples. Compare quantitation dynamic ranges to conventional IHC.
Ib.1 (Davis) Prepare cell culture samples and define standard clinical samples with matched frozen tissue as controls for each antibody.

Completed.
Ib.2 (Davis) Conduct quantitative western blot analysis for cell/ tissue quantitative protein determination for each antibody.
Completed.
Please see Figure 2 Appendix I

Ib.3 (Davis) Prepare matched samples used in western blots (Figure 2 appendix I) for conventional and MIBI IHC.
Completed.
Please see Figure 3 Appendix I

Ib.4 (Davis) Conduct conventional IHC.
Completed.
Ib.5 (Davis) Use Aperio image analysis tools to quantify signal intensity and distribution of conventional IHC.
Pilot testing completed, reoptimized using IMARIS image analysis. Additional tool sets under evaluation.
Please see Figure 4 Appendix I

Ib.6 (Stanford) MIBI imaging of matched samples.
Year 2.
Ib.7 (Stanford) Use MIBI image analysis tools to quantify signal intensity and distribution of the MIBI IHC.
Pilot analyses completed. Test samples begin Year 2.
Ib.8 (Davis) Prepare standard curves of western quantified analyte concentration v. conventional IHC quantitiation.
In progress.
Ib.9 (Davis and Stanford) Prepare standard curves of western quantified analyte concentration v. MIBI IHC.
Year 2.
Ib.10 Reiterate (1-9) with additional samples at high and low concentrations as needed to define the dynamic range limits as needed (find the curve plateaus to determine the full linear detection ranges).
Samples identified, analyses Year 2-3.
Ib. 11 (Davis and Stanford) Report technical applications findings—manuscript.
Year 2-3.

Ic. Automate IHC4 + BAG1 score, and "Mammostrat" score using one slide 13 marker quantitative image. Continue development of the analysis software.
Ic.1 (Stanford) Utilize cytokeratin and/or ECAD channels to segment epithelium from stroma.
Completed.
Please see Figure 5 Appendix I

Ic. 2 (Stanford) CellProfiler segmentation using hematoxylin channel (aluminum peak) or addition of dsDNA antibody if needed (Davis prep, Stanford analysis).
Completed.
Ic. 3 (Stanford) Import segmented multiparemeter data into SPADE software package for population analysis.
In progress.
Ic. 4 (Davis) Develop cell position matrices for aim 3 evaluation.
Year 2.
Ic. 5 (Davis and Stanford) Test display utility, and modify for user/pathology interface.
Year 3.

Ic. 6 (Davis) Use standard curve quantified (ER, HER2) and categorical percentages (PR, KI67) to provide input for IHC4 score algorithm.
Pilot methods completed. Evaluation measurments Year 2.
Ic. 7 (Davis) Use standard curves and categorical percentages to provide input for Mammostrat score algorithm.
Year 3.
Ic. 8 (Davis) Compare output scores to clinically derived conventional scores.
Year 3.
Ic. 9 (Davis and Stanford) Report utility findings—manuscript.
Year 3.

Aim II: MIBI Oncotype mRNA in situ: Develop the multiplex panel of the following 21 gene mRNA in situ hybridization for quantitative analysis and recalculation of the current algorithms for recurrence risk: (16 analytical, 5 controls: Ki67, STK15, Survivin, CCNB1, MYBL2, MMP11, CTSL2, HER2, GRB7, GSTM1, CD68, BAG1, ER, PGR, BCL2, SCUBE2, ACTB, GAPDH, RPLPO, GUS, TFRC)

IIa. Compare hybridization results for mass tagged probe designs from both collaborating companies (ACD and Biosearch). Develop hybridization conditions for mixing probe types.
IIa. 1 (Davis) Choose and prepare FFPE tissue sections and control FFPE cell line pellet sections for hybridizations.
Completed.
IIa. 2 (Davis) Test pre-optimized conditions (from collaborating company data) using conventional fluorescent label detection.
In progress. 5 of 21 targets optimized.
IIa. 3 (Davis) Prepare mass tagged ISH probes.
Year 2.
IIa. 4 (Davis) Prepare tissue samples with mass tagged ISH probes: single label, double label and half panel and full panel.
Year 2.
Ia.5 (Stanford) nanoSIMS MIBI imaging of single, double and panel labeled samples.
Year 2.
Ia.6 (Stanford) Initial image analysis of MIBI images for display of quantitative ISH signals.
Year 2.
Ia.7 (Stanford) Image cell segmentation and cell distributions by ISH phenotype and cell morphology.
Year 2-3.

IIb. Measure quantitative ISH imaging against real-time PCR to develop standard curves across different tissue preparations for each probe. Assess pairwise interference.
IIb.1 (Davis) Prepare cell culture samples and define standard clinical samples with matched frozen tissue as controls for each ISH probe.
Completed.
Please see Figure 3 Appendix I

IIb.2 (Davis) Conduct quantitative RT-PCR analysis for cell/ tissue quantitative mRNA determination for each transcript.
In Progress. 12 of 21 targets quantified.
IIb.3 (Davis) Prepare matched samples used in RT-PCR for MIBI ISH.
Year 2.
IIb.4 (Stanford) MIBI imaging of matched samples.
Year 2.

IIb.5 (Stanford) Use MIBI image analysis tools to quantify signal intensity and distribution of the MIBI ISH.
Year 2-3.
IIb.6 (Davis and Stanford) Prepare standard curves of RT-PCR analyte concentration v. MIBI ISH quantitiation.
Year 2-3.
IIb.7 Reiterate (1-6) with additional samples at high and low mRNA concentrations as needed to define the dynamic range limits as needed (find linear detection ranges).
Year 2-3.
IIb. 11 (Davis and Stanford) Report technical applications findings—manuscript.
Year 3.

IIc. Normalize quantitative ISH imaging using control genes for algorithm development. Compare clinical samples using MIBI Oncotype mRNA *in situ* to Oncotype DX recurrence score.
IIc.1 (Stanford) Compute average intensity/dot count for each analyte over the area of tumor.
Year 2-3.
IIc. 2 (Stanford) Compare computed average to qRT-PCR values.
Year 2-3.
IIc. 3 (Stanford) Normalize values with control probes for input into algorithm.
Year 2-3.
IIc. 4 (Davis) Reverse engineer an *in situ* Oncotype DX recurrence score by comparing to clinically derived (deidentified) score values across multiple tumors.
Year 2-3.
IIc. 5 (Davis) Validate *in situ* recurrence score against an additional test set and define the variance parameters.
Year 2-3.
IIc. 6 (Davis) Determine features associated with standard v. *in situ* score discrepancies.
Year 2-3.
IIc. 7 (Davis and Stanford) Report utility findings—manuscript.
Year 3.

Aim III: Heterogeneity as an additional tumor virulence measure: The data generated in aims I and II above provide a complex matrix with each analyte quantity per cell as well as cell morphology and size information, as well as microanatomic location information. Aim III will examine computational approaches to assess heterogeneity.

IIIa: Finding minority populations of virulent cancer cells. Do small numbers of cells with high risk calculations embedded in otherwise low risk tumors imply a greater risk?
IIIa. 1 (Stanford) Use CellProfiler with both MIBI IHC and MIBI ISH data to identify subsets of cells with “high scores” or “low scores”.
Year 3.
IIIa. 2 (Davis) Construct score histograms of tumor cell populations to compare distributions across multiple breast cancer phenotypes.
Year 3.

IIIb. Multiparameter topology assessment: Using more advanced statistical methods like principal component analysis taking into account not just individual cell paramenters, but molecularly defined populations proximity and relationship to the tumor shape and intersection with the surrounding tissue structures.
Year 3.

Notes: *For this reporting period describe: 1) major activities; 2) specific objectives; 3) significant results or key outcomes, including major findings, developments, or conclusions (both positive and negative); and/or 4) other achievements. Include a discussion of stated goals not met. Description shall include pertinent data and graphs in sufficient detail to explain any significant results achieved. A succinct description of the methodology used shall be provided. As the project progresses to completion, the emphasis in reporting in this section should shift from reporting activities to reporting accomplishments.*

B. What opportunities for training and professional development has the project provided? *Nothing to Report.*

C. How were the results disseminated to communities of interest? *Nothing to Report.*

D. What do you plan to do during the next reporting period to accomplish the goals? Outlined in part A above.

E. CHANGES/PROBLEMS: So far, the project is progressing without major problems. Several minor issues, such as choice of image analyses software have resulted in minor changes to our plans, but nothing significant. One major difficulty has been obtaining test ISH probes from some of the industry providers. The Material Transfer Agreements (MTAs) have taken longer than anticipated to finalize.

F. PRODUCTS: *Nothing to Report.*

G. PARTICIPANTS & OTHER COLLABORATING ORGANIZATIONS

Name	Alexander Borowsky
Project Role	Principle Investigator
Researcher Identifier	N/A
Person Months Worked	1
Funding Support	This award

Name	Richard Levenson
Project Role	Co-Investigator
Researcher Identifier	N/A
Person Months Worked	1
Funding Support	This award

Name	Hidetoshi Mori
Project Role	Technician
Researcher Identifier	N/A
Person Months Worked	11
Funding Support	This award

Conclusion

In conclusion, at the time of this first year progress report, planned work objectives are progressing on schedule. The bulk of the first year of work occurred at UC Davis, but critical peripheral work including the design and assembly of a new secondary ion mass spectrometer (not funded by this study) have been completed at Stanford. We anticipate continued progress toward the goals of this proposal in the coming years.

References and Appendices:

Appendix I Figures from UC Davis.

Immunohistochemistry and mass spectrometry for highly multiplexed cellular molecular imaging.
Levenson RM, Borowsky AD, Angelo M.
Lab Invest. 2015 Apr;95(4):397-405. doi: 10.1038/labinvest.2015.2. Epub 2015 Mar 2. Review.
PMID: 25730370

Multiplexed ion beam imaging of human breast tumors.
Angelo M, Bendall SC, Finck R, Hale MB, Hitzman C, Borowsky AD, Levenson RM, Lowe JB, Liu SD, Zhao S, Natkunam Y, Nolan GP.
Nat Med. 2014 Apr;20(4):436-42. doi: 10.1038/nm.3488. Epub 2014 Mar 2.
PMID: 24584119

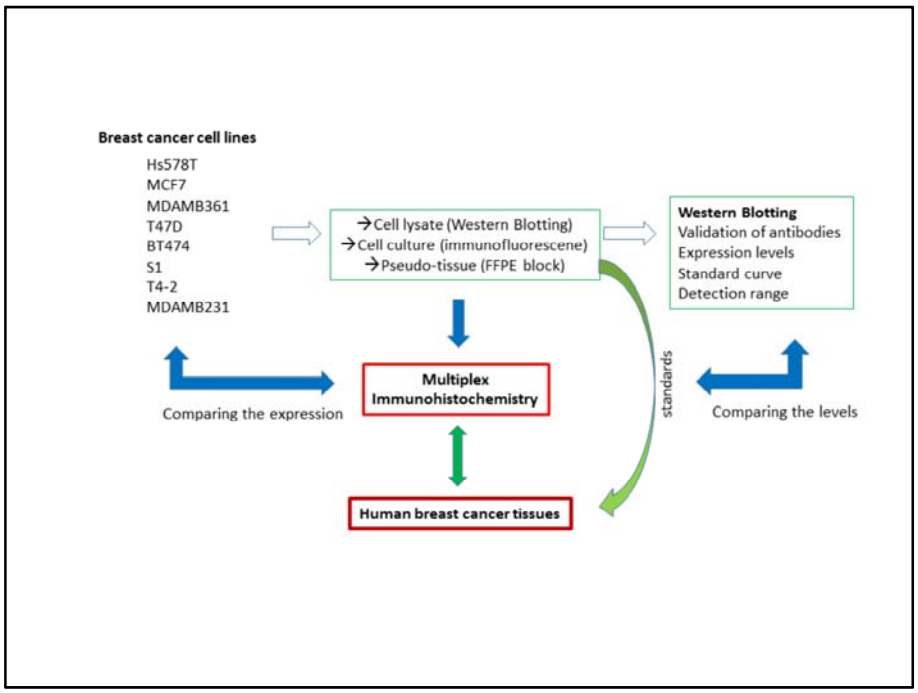

Fig.1. Scheme of multiplex immunohistochemistry project.
Scheme is showing that a sample preparation for validating antibodies by western blotting (WB), immunofluorescence and formalin-fixed paraffin-embedded peudo-tissue made from each breast cancer cell line. These samples are tested to validate antibody availability for immunohistochemistry before it is tested on human breast cancer tissue samples.

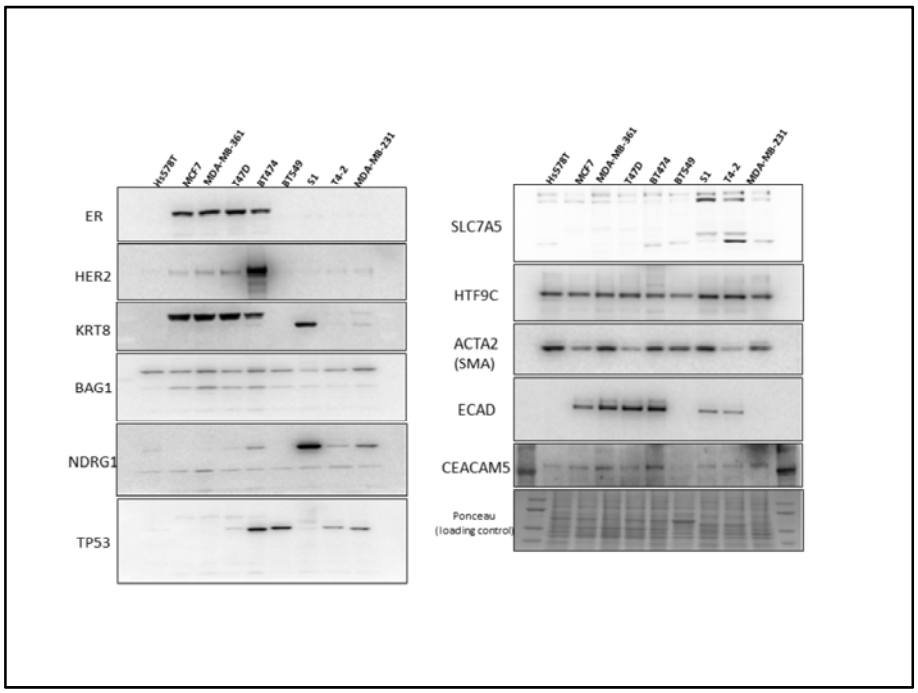

Fig.2. Validation of antibody by Western Blotting.
Each antibody available for Western Blotting was tested with cell lysate of each breast cancer cell line.

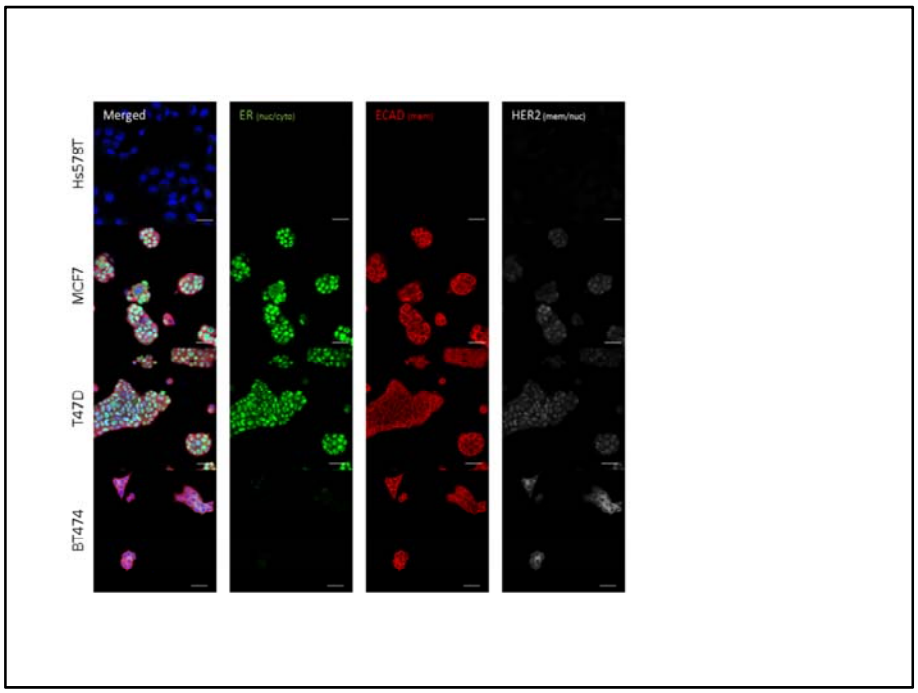

Fig.3. A test of multiplexed immunohistochemistry (IHC) on formalin-fixed breast cancer cells.
Breast cancer cell lines (Hs578T, MCF7, T47D and BT474) were cultured on glass slide and immunostained with ER, ECAD and HER2 by performing IHC with Tyramide-based signal amplification.

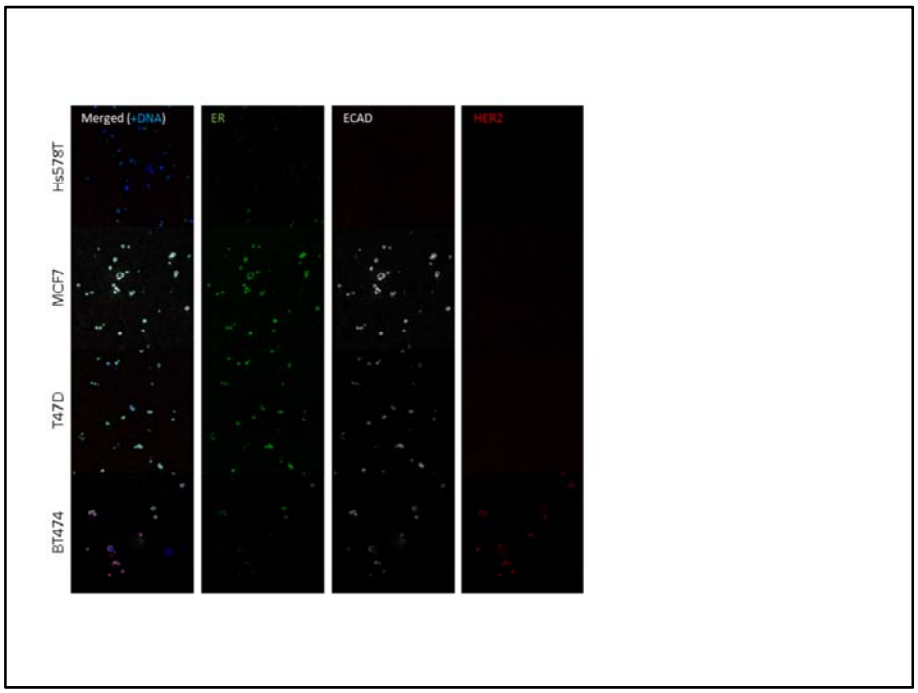

Fig.4. A test of multiplexed immunohistochemistry (IHC) on tissue sections of FFPE pseudo-tissue with breast cancer cells.
Pseudo-tissue section was prepared from breast cancer cell lines (Hs578T, MCF7, T47D and BT474) embedded in type-I collagen gel which was fixed with formalin and infiltrated with paraffin.
Signal for each marker was detected with anti-ER, -ECAD and -HER2 by performing IHC with Tyramide-based signal amplification.
This experiment confirmed that each antibody works effectively for IHC on FFPE tissue sections.

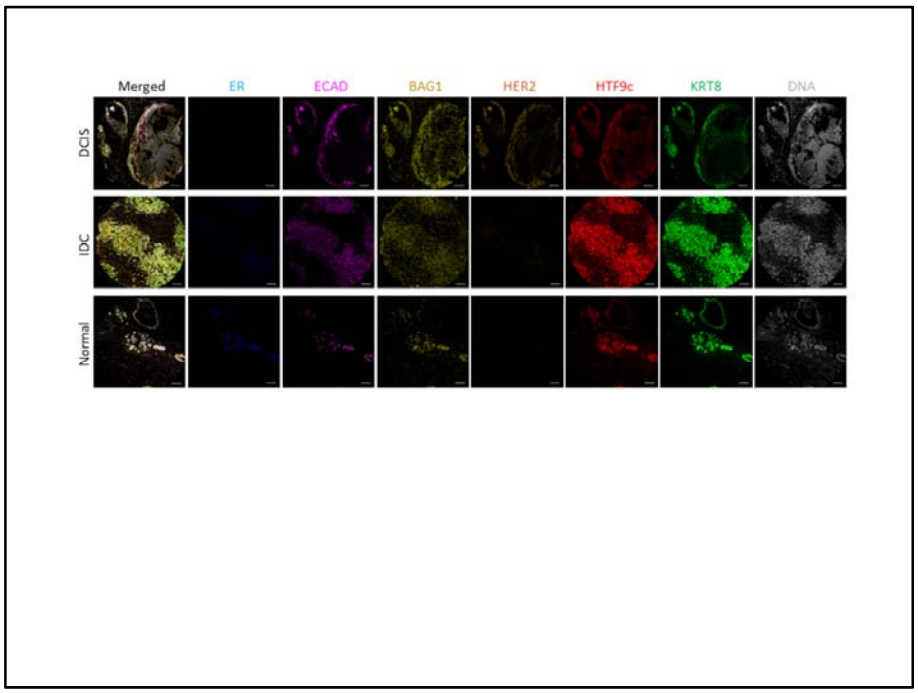

Fig.5. 7-color multiplex IHC imaging on human breast cancer tissues.
7-color (6 markers and DNA staining) was performed on tumor microarray cores of FFPE treated breast cancer tissues.

Figure 1. The following set of images, obtained using the new MIBI device designed by Dr. Michael Angelo and Dr. Sean Bendall, and imaged in the Angelo lab at Stanford, demonstrates the multiplexing capabilities of the MIBI. This is an 18-plex image.

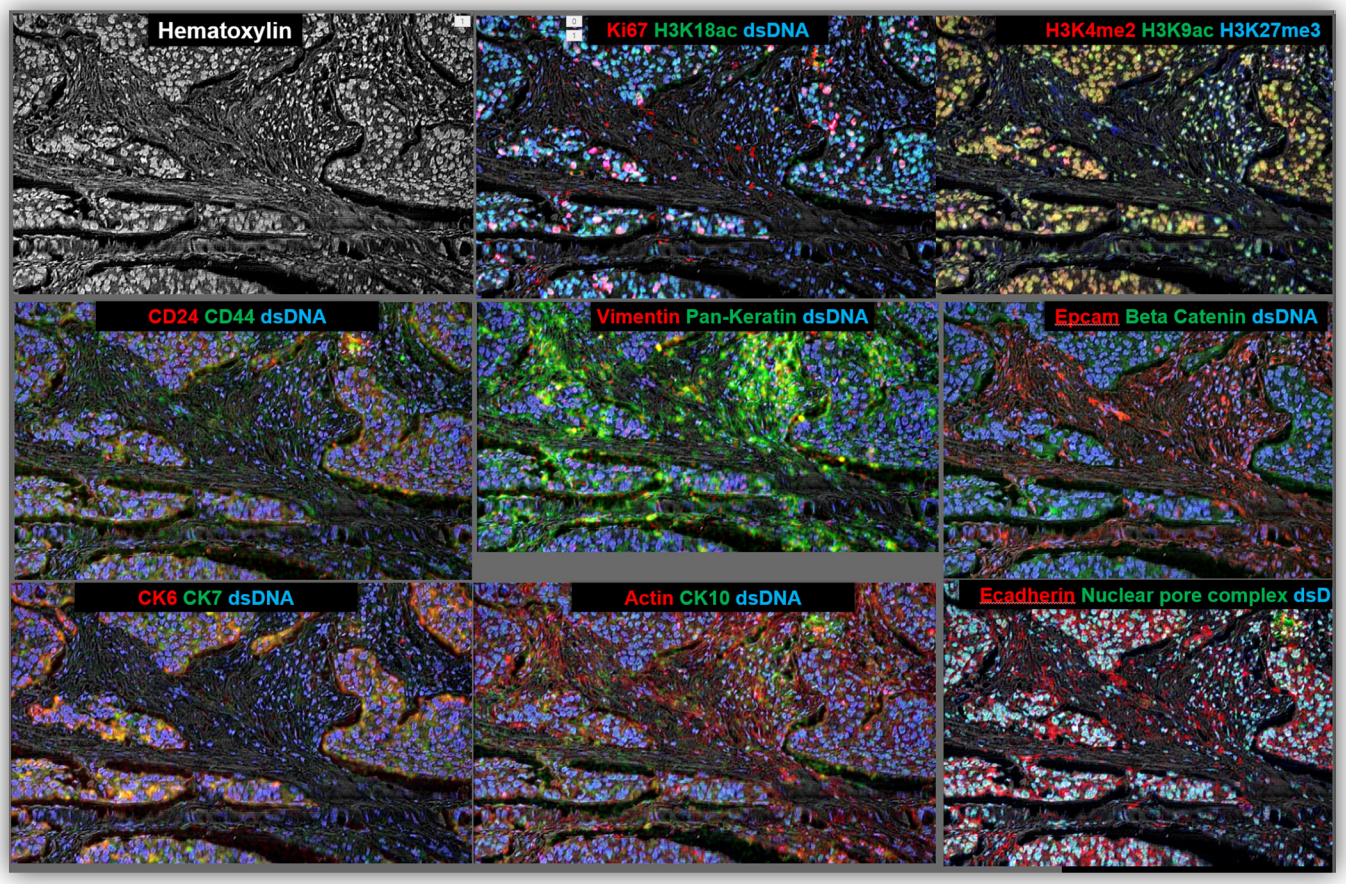

Figure 2. – CODEX analysis of mouse spleen cryosections co-stained for 28 antigens.

(A), (B) Three levels of magnification of 28 color CODEX staining of normal spleen. Three collated images on the top left correspond to the legend of antibody renderings per cycle, gross morphology photograph of MRL/lpr (left) and normal (right) spleen embedded in O.C.T. block prior to sectioning and montage of antibody renderings in all 14 CODEX cycles at high resolution. Red color corresponds to antibodies rendered by extension with dUTP-Cy5, green – dCTP-Cy3. All images are derived from a single scan with a 20x air objective of an area covered by 47 tiled fields. **(C)** staining of MRL/lpr spleen sections with same panel as in (A). Due to much larger area of the MRL/lpr spleen cross-section two characteristic regions together occupying same area as the normal spleen sample were imaged and jointly quantified. **(D)** Comparing cytometric data obtained by regular fluorescent flow cytometry (top row) with quantification from segmented CODEX images (bottom row) **(E)** Top two panels show heatmaps depicting the likelihood probability of a cell type to be within a vicinity of another cell type within a normal (top panel) spleen or MRL/lpr (middle panel heatmap) spleen. Bottom panel is a fraction bar blot showing changes in percentages of each cell type computationally identified in CODEX spleen data. Asterisk marks the DN T-cells vastly exceeding the normal numbers in MRL/lpr spleen.

Thus, we have developed the means, when MIBI imaging is ready, to appropriately segment high dimensional images.

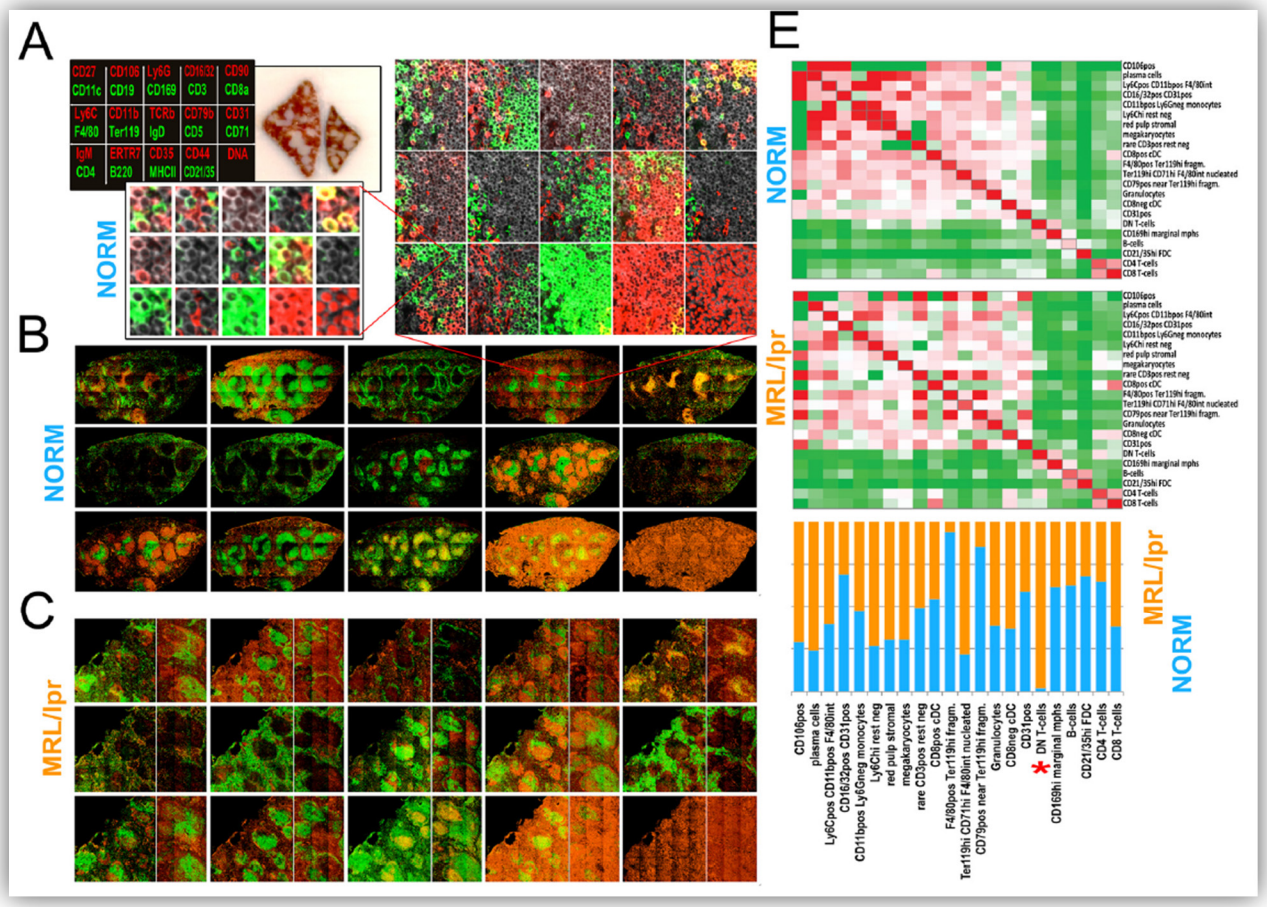

Figure 3. CODEX analysis of mouse spleen cells co-stained for 22 antigens.

(A) Montage of a fragment of imaging field of the 11 cycles of CODEX used to render the staining of mouse cells with 22 antibodies. TCEP cycles were omitted from the montage. First cycle corresponds to top left and last to bottom right. Right most bottom image shows cells pseudo-colored according to expression of all 22 antigens. Each antigen/cycle corresponds to a color from spectrum palette. Under each field of view is a biaxial corresponding to co-expression analysis of the antigens of the antigens measured in this cycle in all cells **(B-C)** Divisive marker trees using Vortex derived data for spleen (B) and bone marrow (C) produced by X-shift analysis of 22-dimensional CODEX dataset. Callouts contains biaxial plots for characteristic antigens for selected population identified in X-shift analysis of 22-dimensional CODEX data. This is a preliminary run for data analysis by imaging.

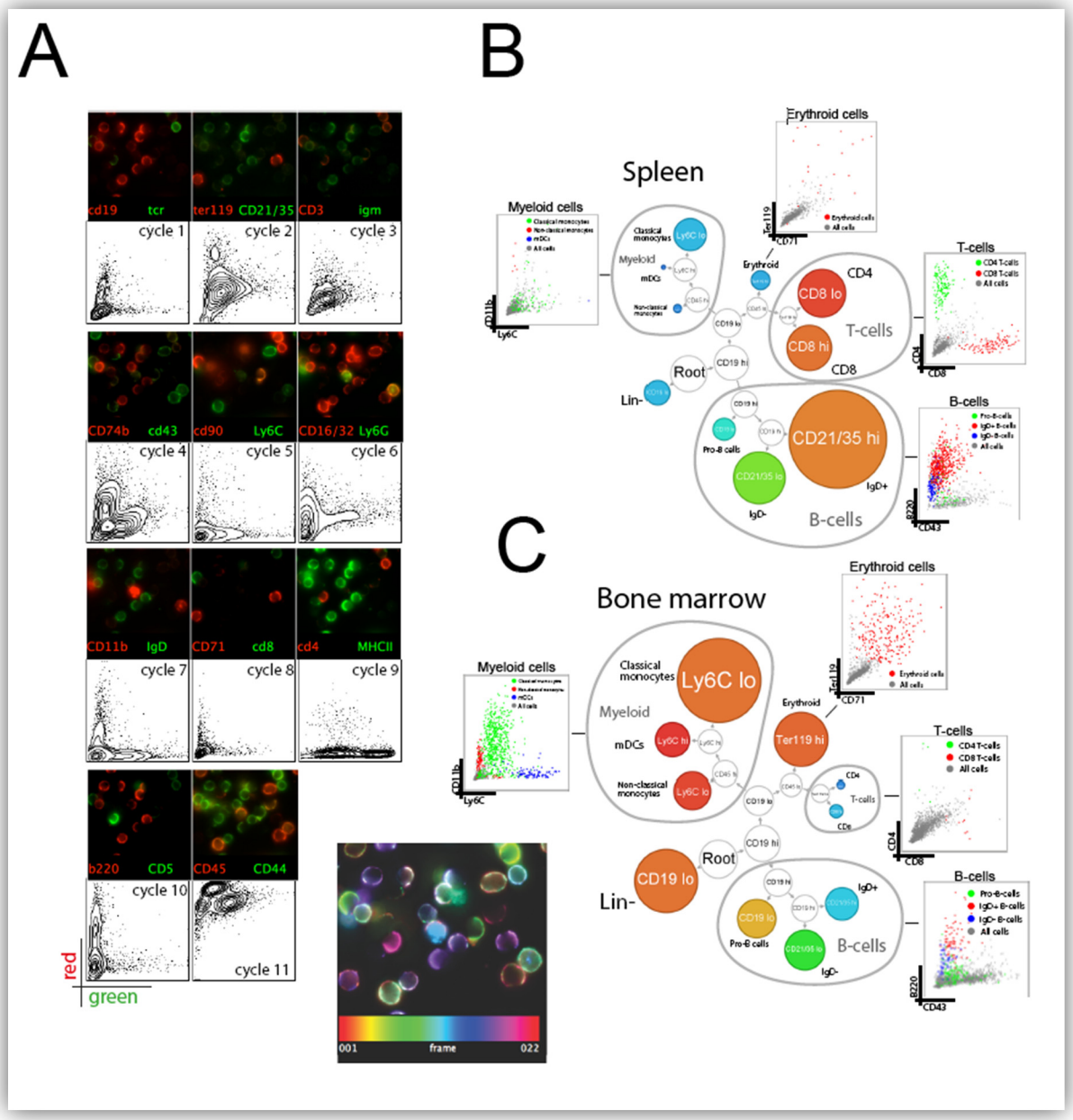

Laboratory Investigation (2015) 95, 397–405

PATHOBIOLOGY IN FOCUS

Immunohistochemistry and mass spectrometry for highly multiplexed cellular molecular imaging

Richard M Levenson[1], Alexander D Borowsky[1] and Michael Angelo[2]

The role of immunohistochemistry (IHC) in the management of cancer has expanded to provide improved diagnostic classification, as well as guidance on disease prognosis, therapy, and relapse. These new tasks require evaluation of an increasing number of protein targets; however, conventional multiplexing, usually achieved using serial tissue sections stained for a single analyte per slide, can exhaust small biopsy specimens, complicate slide-to-slide protein expression correlation, and leave insufficient material for additional molecular assays. A new approach, mass spectrometry immunohistochemistry (MSIHC), compatible with high levels of target multiplexing and suitable for use on formalin-fixed, paraffin-embedded samples can circumvent many of these issues. The strategy employs antibodies that are labeled with elemental mass tags, such as isotopically pure lanthanides not typically found in biological specimens, rather than with typical fluorophores or chromogens. The metal-labeled antibodies are then detected in tissue using lasers or ion beams to liberate the tags for subsequent mass spectrometry detection. Within a given multiplexed IHC panel, the metal labels are selected so that their respective masses do not overlap. More than 30 antibodies have been imaged simultaneously, and up to 100 antibodies could potentially be detected at once if the full available mass spectrum is deployed. MSIHC has a number of advantages over conventional IHC techniques. Background due to autofluorescence is absent and the dynamic range is 10^5, exceeding immunofluorescence and chromogenic IHC by 100-fold and 1000-fold, respectively. Detection of labeled primary antibodies improves assay linearity over both chromogenic and fluorescent IHC. Multiplexed mass-tagged antibodies incubated simultaneously with tissue do not appear to cross-interfere, and because the mass tags do not degrade, samples are stable indefinitely. The imaging resolution of multiplexed ion-beam imaging can be better than light microscopy. With appropriate instrumentation, MSIHC has the potential to transform research and clinical pathology practice.

Laboratory Investigation (2015) **95,** 397–405; doi:10.1038/labinvest.2015.2; published online 2 March 2015

Next-generation sequencing, quantitative PCR, and gene expression arrays have demonstrated the usefulness of methods that can examine tens to thousands of genes from tissue extracts. These non-imaging approaches have, however, increased demands for *imaging* methods that might be capable of generating equivalent levels of information at scales spanning tissue-level to the subcellular. There are good reasons to try to meet this challenge, as non-imaging-based multiplexed assays are unable to address many important questions in pathobiology. These bulk sample analyses are largely uninformed by spatial context and may convey only limited information on possibly important minority cell populations, as phenotypes arising from predominant cellular components often obscure signals from low-abundance but possibly important cell subsets. Such minority populations, of course, can be of great interest, as in the case of cancer stem cells thought to represent a small but critical part of a tumor ecosystem.[1,2] In addition, a highly multiplexed imaging platform could be used to understand the interplay of intra- and inter-cellular signaling pathways by examining how phenotypically distinct cell populations are spatially distributed relative to one another.

The role of immunohistochemistry (IHC, antibody-based protein detection in cells and tissue sections) in the clinical diagnosis of cancer has expanded greatly in recent years to provide critical information about disease prognosis, therapy, and relapse. These new tasks require the determination of abundance and subcellular location of an increasing number of

[1]Department of Pathology and Laboratory Medicine, UC Davis Medical Center, Sacramento, CA, USA and [2]Department of Pathology, Stanford University, Palo Alto, CA, USA
Correspondence: Dr RM Levenson, MD, Department of Pathology and Laboratory Medicine, UC Davis Medical Center, 4400 V. Street, Suite 1112, Sacramento, CA 95817, USA.
E-mail: levenson@ucdavis.edu

Received 31 October 2014; revised 23 December 2014; accepted 24 December 2014

proteins within a single biopsy, and this is accomplished using either brightfield (chromogenic) or fluorescence detection techniques. Both have limitations. Chromogenic staining in clinical labs is typically performed using a single primary antibody at a time, with additional protein targets being visualized in separate serial biopsy sections. This technique relies on multivalent secondary antibodies conjugated to enzymatic reporters, such as horseradish peroxidase, that generate colored pigments by reacting with a substrate, such as 3,3′-diaminobenzidine. Although two or more targets can be visualized simultaneously using different chromogens and amplification schemes, colorimetric detection of more than three antigens using multiple enzyme-linked secondary antibodies is challenging.[3] In practice, chromogenic multiplexing is usually limited to two targets because of difficulties encountered in sample preparation and imaging. Beyond this relatively low multiplexing ceiling, IHC has additional shortcomings.[4] Chromogenic IHC staining can generate dense deposits that are easy to detect but difficult to quantitate, because of nonlinear optical effects and low achievable dynamic ranges. These issues are compounded when using multiple contrast agents in a single tissue section; multiple pigments layered on top of one another may generate regions within the tissue that are virtually opaque and cannot be transilluminated.

On the other hand, fluorescent labels used in immunofluorescence (IF)-based techniques can provide a higher signal-to-noise ratio than chromogenic labels and are more frequently used for simultaneous detection of multiple targets; nevertheless, they present their own challenges. Practical limitations include a typical requirement for the use of separate animal species for each primary–secondary antibody pair, and for substantially non-overlapping reporter emission spectra if multispectral imaging techniques are not available.[5–8] It should be noted that impressive levels of multiplexing (up to 10 labels at a time) are possible using conventional fluorescence microscope equipment, but this requires careful matching of fluorescent reporters, dichroic mirrors, and band-pass filters along with a complicated repertoire of species- and subtype-matched primary and secondary antibodies (Trajan Maric, personal communication). Thus, conventional IHC (IF) methodologies are not capable of generating the robust multiplexed, quantitative data needed to understand the relationship between tissue microarchitecture and expression at a proteomic level.

These and similar challenges have led to efforts that extend the multiplexing capabilities of IF markedly, albeit with some logistical hurdles. One of the most technically successful approach has used sequential methods for multiplexing, sometimes referred to as 'dye-cycling,' that involve repeated cycles of primary staining (with or without secondary staining), imaging, and then quenching or removing each cycle's fluorescent reporter. Methods for erasing the signals have included low-pH antibody elutions, high-temperature fluorophore denaturation, antibody stripping, and photobleaching.[9–16] Recently, a system ('MultiOmyx™') using dye-cycling has been commercialized by GE Healthcare and deployed for a few clinical indications.[17] Because of the serial steps that have to be performed, the throughput is relatively low, and as with all complicated procedures, quality assurance or validation remains a challenge. Finally, it is worth stating that fluorescence imaging, however accomplished, has some intrinsic limitations. These include moderate sensitivity and dynamic range,[18] problems with autofluorescence background, variable reagent and specimen stability, varying quantum yields,[19] and potential channel cross-talk.[20]

Nevertheless, IHC and IF imaging techniques provide unique biological information that in many cases cannot be attained by other methods. Single cells can be visualized with signal fidelity equal to that achievable in the bulk population, such that even rare cell populations can be studied. Individual Hodgkin's cells can be detected and easily characterized against a dense inflammatory background, a clinically relevant indication.[21] All components of an important and complicated microenvironment can be examined simultaneously, providing insight into biological cross-talk present at the tumor–host interface. Perhaps most importantly, the spatial precision of these techniques spans many orders of magnitude, from the subcellular level up to whole organs. The value of such spatial precision increases significantly when multiple proteins can be detected simultaneously and protein co-expression or interaction can be evaluated.

Recent reports of mass spectrometry immunohistochemistry, as described in *Nature Methods* and *Nature Medicine*,[22,23] have outlined a new approach for achieving simultaneous, high-order multiplexed imaging while avoiding requirements for extended labeling and/or multiple imaging sessions. In the place of fluorophores, both methods use antibodies labeled with isotopically pure metal chelator tags. Such an approach overcomes the limitations of spectral overlap seen with fluorophores, with the narrow and potentially completely resolvable peaks derived from mass measurements of the metals (Figure 1). The two methods differ in how these tags are liberated from the sample, ionized, and detected. Scanning mass cytometry (SMC) is a form of laser-ablation inductively coupled plasma time-of-flight mass spectrometry that uses a high-intensity laser with spot sizes down to 1 μm to liberate tissue into a carrier gas. The carrier gas transports the ablated sample into an argon plasma where it is ionized and subsequently detected. The second technique, multiplexed ion-beam imaging (MIBI) is based on secondary ion mass spectrometry (SIMS) in which the sample is scanned by an ion beam with a sub-micron spot size. The secondary ions that are released are then detected using a magnetic sector mass spectrometer (Figure 2). Using these novel labeling and detection strategies, simultaneous detection of 40 and potentially up to 100 targets can be achieved in formalin-fixed, paraffin-embedded tissue sections, the most common sample type in clinical repositories worldwide.[24]

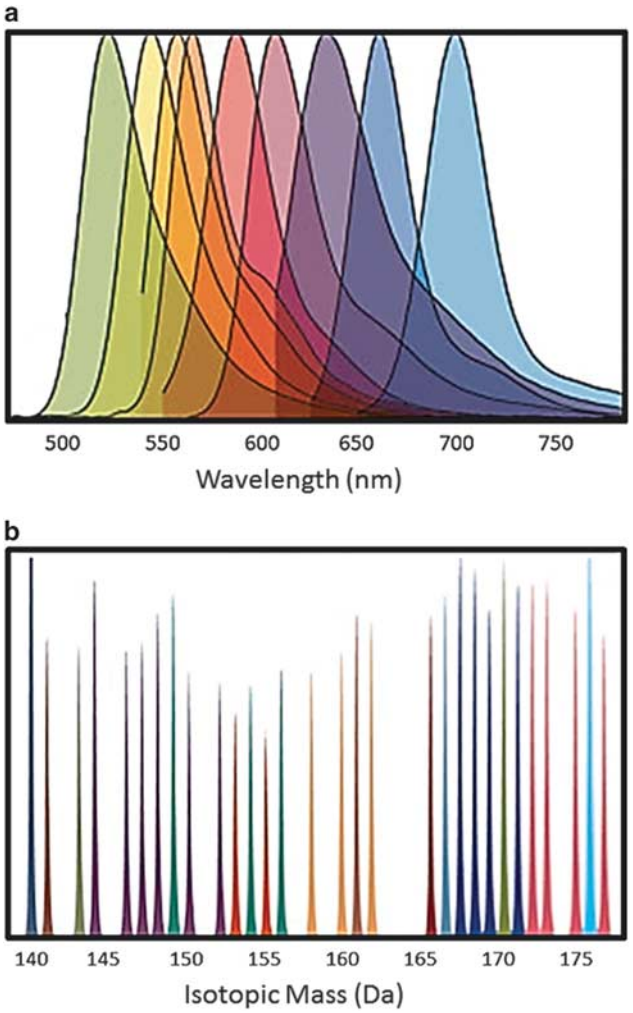

Figure 1 Comparison of overlap potential between fluorophores and metal tag labels. The top panel (**a**) indicates the spectra of commonly used fluorophores emitting in the visible range. As can be seen, there is considerable overlap between adjacent and even substantially separated fluorescent emissions. Such overlap can be resolved with the use of carefully designed excitation and emission filters and/or with spectral imaging, but does limit the potential for high-level multiplexing. In contrast, the metal tags (lower panel, **b**) have masses that can be clearly separated with either magnetic sector or time-of-flight-based mass spectrometers, opening up the possibility of multiplexing as many as 100 or so analytes simultaneously.

This ability to visualize the presence, abundance, location, and functional state of so many targets in cells and tissues simultaneously has been described as a true next-generation approach in IHC.[25] Important from a practical perspective, all the labels can be applied in a single incubation step, and, with the right instrumentation, can then be detected during a single imaging procedure. However, such a procedure implies that a single antigen retrieval protocol will be adequate for all targets, but this may not necessarily be true for every panel attempted.

Current implementations of both methods have strengths and weaknesses. The maximum field of view before stage movement of SMC is up to 500 μm^2, whereas the maximum field of view using MIBI is limited to approximately 100 μm^2. Because SMC utilizes TOF detection, all targets are measured simultaneously. In contrast, MIBI *currently* uses magnetic sector detection, which allows only seven targets to be detected per scan; the mass sensors have to be re-positioned to detect new targets for each additional scan. On the other hand, the overall ionization yield with MIBI ranges between 1% and 10% depending on the isotopic tag, and the sensitivity of MIBI is thus predicted to be around 100 times higher than SMC, in which ionization yields are approximately 0.01%. The resolution of MIBI is currently 200 nm, compared with 1 μm for SMC. Last, where SMC is destructive and ablates the full sample thickness, sample scanning by MIBI only consumes the top 5–10 nm of sample, permitting survey and replicate scanning, and potentially high-resolution axial (depth) imaging as well. Of course, both techniques are under active development, and their properties may change substantially in the future. As our expertise centers around MIBI, the following discussion will focus on how this method has been used and what innovations can be anticipated.

MATERIALS AND METHODS

MIBI analysis is currently being performed using the NanoSIMS 50L secondary ion mass spectrometer from Cameca (Gennevilliers, France). Samples are mounted in a sample holder, loaded into a vacuum chamber and raster-scanned with a primary ion beam. The impact of this ion beam liberates secondary ions present on the sample surface, and these are subsequently identified and quantified via a magnetic sector mass spectrometer. In the case of multiplexed IHC, samples are scanned with a negatively charged oxygen (O^-) duoplasmatron source, which liberates lanthanide adducts of the bound antibodies as positively charged secondary ions. Because the spot size of the current duoplasmatron source is adjustable down to 200 nm, image resolution is on par with standard light microscopy. A positively charged cesium liquid metal ion gun can also be used to measure negative secondary ions, such as carbon, nitrogen, oxygen, and halogens. Current liquid metal ion gun sources are adjustable down to spot sizes of 50 nm, permitting ion imaging with lateral resolution that is at least equivalent to that of confocal microscopy, and because of MIBI's 5- to 10-nm ablation depth per scan, should outperform confocal systems in terms of axial resolution. This method can be used to visualize the distribution of isotopically labeled metabolic reporters, such as ^{15}N-labeled amino acids or nucleotides, and has been employed elegantly in previous work by others to track protein turnover within the tips of stereocilia in the inner ear and to visualize cardiomyocyte cell turnover.[26–28] These impressive results are due in part to the ability of SIMS to achieve parts-per-billion sensitivity with a dynamic range of 10^5.[27,29,30]

As noted, MIBI is capable of lateral (x,y) resolution comparable to light microscopy, with *sensitivity* that appears to be

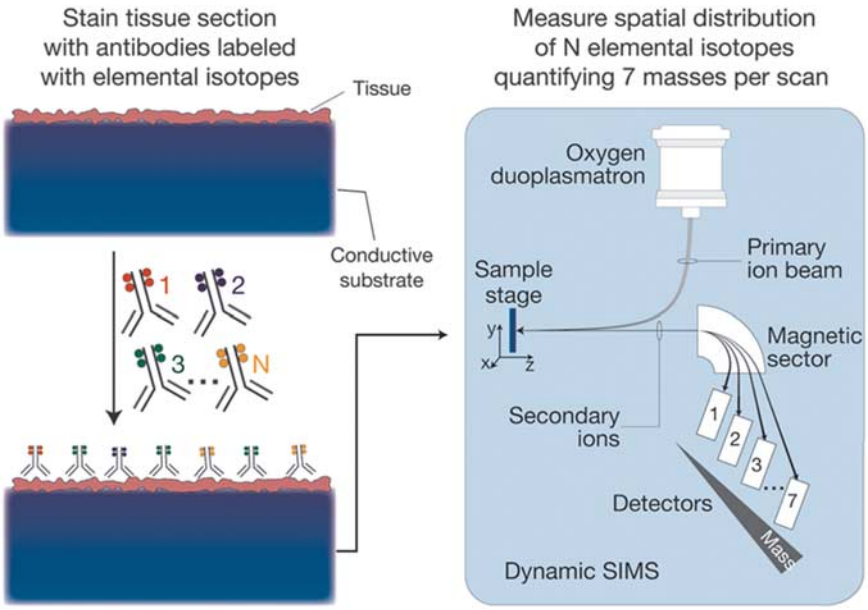

Figure 2 MIBI sample preparation and scanning procedures. Biological specimens, such as FFPE tissue or cell suspensions, are immobilized on a conductive substrate, such as indium tin oxide-coated glass or silicon wafer. Samples are subsequently stained with antibodies conjugated to unique transition element isotope reporters, dried, and loaded under vacuum for MIBI analysis. The sample surface is rasterized with a primary ion beam (O^-) that sputters the antibody-specific isotope reporters present on the sample surface as secondary ions. Metal-conjugated antibodies are quantified via replicate scans of the same field of view, during which up to seven metals reporters are measured with each scan (figure courtesy *Nature Medicine*).[23]

equal to or greater than conventional IF and a *dynamic range* that may exceed that of IHC by as much as three orders of magnitude. However, one major obstacle to broader use of this platform is its current throughput. Analysis of a 1-mm^2 area of tissue at 200 to 300 nm resolution stained with seven markers currently takes 6–7 h, far too slow to be amenable to routine clinical use. However, next-generation primary ion sources, application-specific scanning routines, enhanced metal-labeling density, and time-of-flight (rather than magnetic sector) detection are projected to reduce acquisition times by 3–5 orders of magnitude while increasing the number of simultaneously detectable species to 50–100 targets. Scan routines employed in our proof-of-principle experiments used beam spot sizes of 200 nm. Alternatively, high-resolution scanning could be restricted to regions of interest identified in preliminary survey scans performed using beam diameters 2 μm or larger (equivalent to a 4X-view). A 10-fold increase in spot size would thus reduce scan time by an additional 100-fold. Acquisition times can be further reduced by increasing the amount of metal attached to each antibody. Current conjugation protocols achieve labeling efficiencies of 100–200 metal atoms per antibody. Work is underway to develop new methods that use branch-chain DNA amplification or nanoparticles that should enable attachment of up to 10 000 metal atoms per antibody. The resulting improved sensitivity and dynamic range with these mass-spec methods should enable better quantitation, as well as opening up the possibility for using lower concentrations of antibodies in some situations.

Examples

Work published in *Nature Medicine*[23] provides some examples of MIBI imaging. Figure 3 displays a small focus of intraductal breast carcinoma from a section of FFPE material stained with hematoxylin and a number of metal-tagged antibodies, and imaged via MIBI. The panels shown are *not* photomicrographs—instead, they were generated by displaying the point-by-point intensity of the mass labels as detected by the magnetic sector sensor, using colors that recapitulate traditional 3,3′-diaminobenzidine-based IHC. The top left panel reflects measurement of actual hematoxylin (ie, not a surrogate stain) abundance, as hematoxylin fortuitously can be directly detected using MIBI because of the high aluminum content present in most hematoxylin preparations. Figure 4 displays a panel of eight antigens detected (out of a complete set of 10 in this imaging session), from three different breast cancer specimens with varying molecular phenotypes. The phenotypes listed down the left border of the image were previously established using standard IHC procedures, and it can be seen that they are recapitulated in the MIBI results shown in the respective image panels. For each tumor specimen, the results are displayed as simulated IF (higher row) or as simulated IHC (lower row). In the case of the simulated IF images, nuclei, highlighted in red, are detected using an antibody directed against double-stranded DNA. Subcellular distribution of all the detected antigens is consistent with their behavior when visualized with conventional imaging methods.

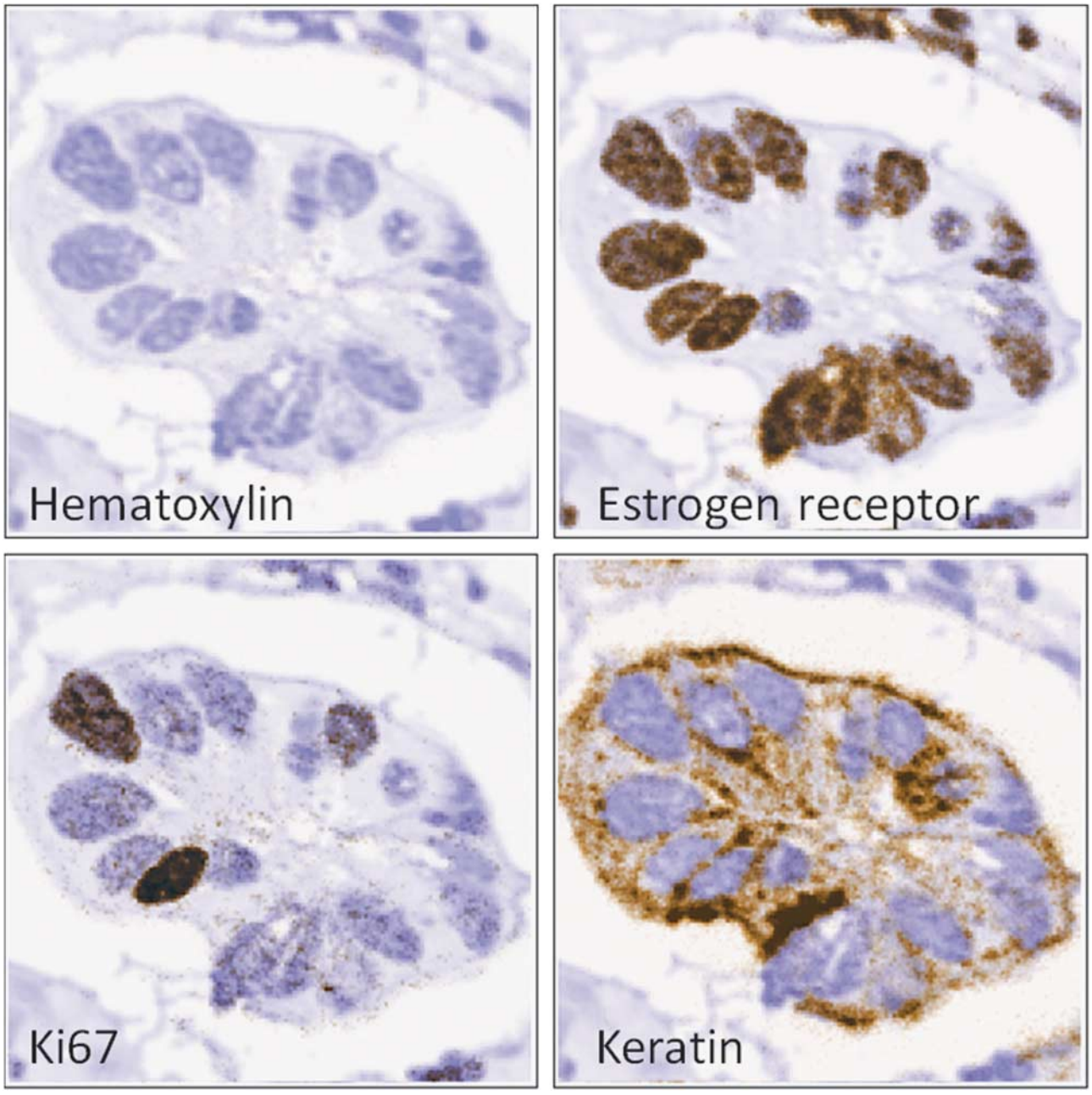

Figure 3 MIBI imaging of FFPE breast cancer. The four panels represent four views of a sample of a FFPE-prepared and multiply labeled specimen of intraductal carcinoma of the breast, obtained during a single scan. The top left panel displays hematoxylin abundance—as the hematoxylin preparations contained aluminum and was consequently detectable by MIBI. The other three panels show the signals of metal-labeled antibodies against ER-alpha, Ki67 and cytokeratin (8/18), commonly interrogated proteins in cancer workups. The metal signals are colored brown and overlain over the hematoxylin signal, colored blue, to replicate the appearance of conventional 3,3′-diaminobenzidine IHC. Field of view = 80 μm^2.

DISCUSSION

Current breast cancer diagnosis and tissue-based analysis include predictive assays to guide therapy decisions, involving a minimum of three analytes: estrogen receptor (ER), progesterone receptor (PR), and HER2. ER and PR IHC long ago supplanted chemical assays for predicting response to anti-hormonal therapies, owing to improved sensitivity and specificity, with analyses that could be verified to reflect the invasive carcinoma separately from any *in situ* or benign areas. Ultimately, however, a very low threshold for positivity was set, even though greater ER expression (higher levels and higher percentages) clearly predicts a higher chance of response.[31] Her2/ERBB2 IHC quantitative assays identify tumors more likely to respond to trastuzumab (Herceptin).

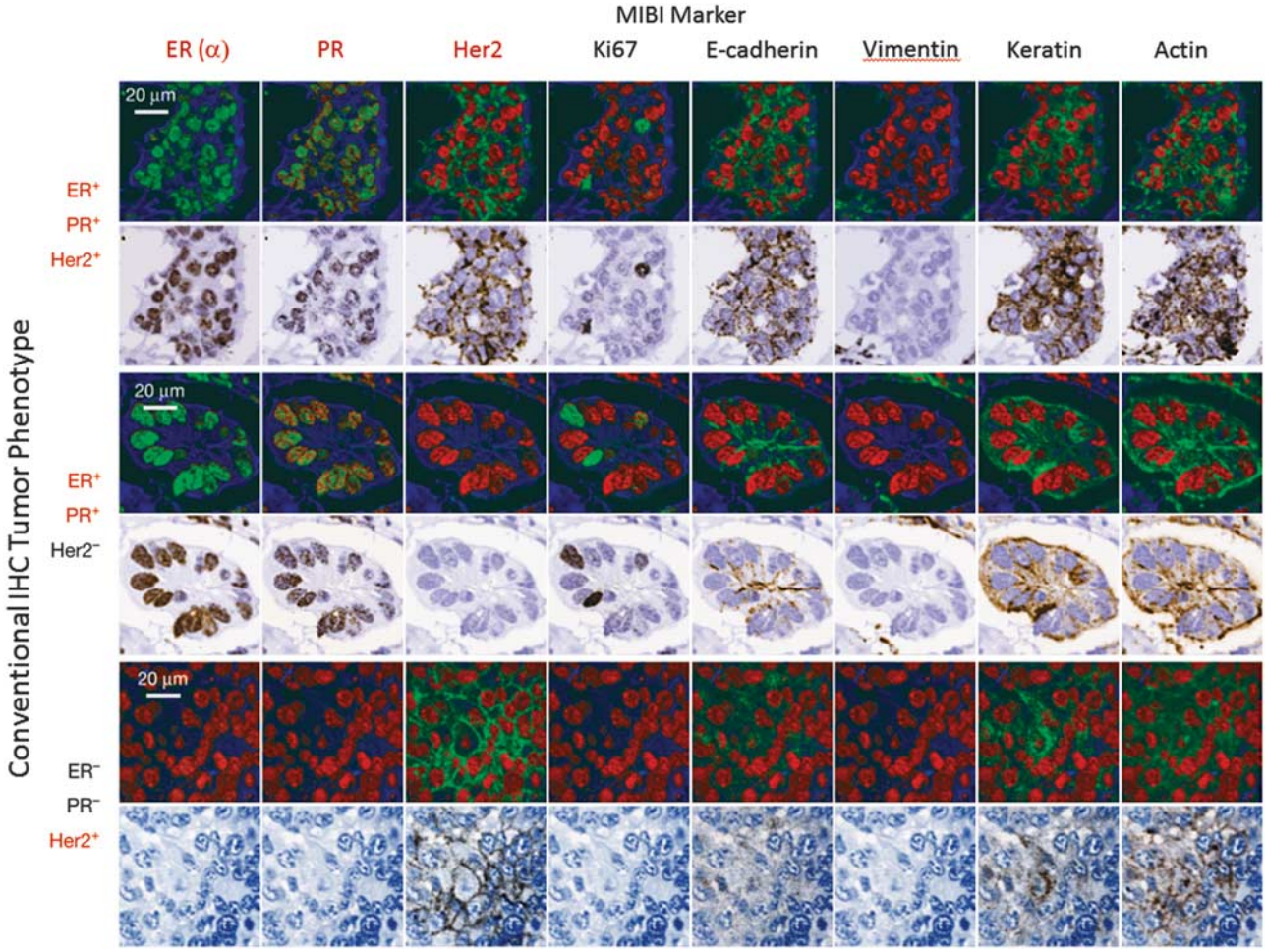

Figure 4 Ten-plex imaging of human breast tumors using MIBI (eight markers shown). Ten antibodies along with hematoxylin signals were used to generate the images in this figure. Eight antibody signals are shown, and the intensities displayed in both fluorescence and brightfield modes. FFPE tissue sections from three different patients were analyzed. The analytes all displayed their anticipated cell-type and subcellular distributions: HER2, ER, and PR are expressed appropriately with respect to the known immunophenotype of each specimen (shown on the left margin). ER-alpha, PR, and Ki67 demonstrate well-demarcated nuclear positivity, whereas e-cadherin and HER2 are membranous; actin, cytokeratin (8/18), and vimentin are cytoplasmic. Keratin is found in the epithelial cells while vimentin is located in the adjacent stromal tissue. Field of view = 80 μm^2 (figure courtesy *Nature Medicine*).[23]

Her2/ERBB2 protein is present on all benign breast epithelium, so that the IHC assay must be carefully controlled to provide a quantitative signal in addition to assessment of a circumferential membranous staining pattern. The nonlinear chemistry of conventional IHC with secondary antibodies and amplified signals has produced an ongoing need for extensive control and validation of the Her2 IHC.[32] Ki67 shows an even greater inter-laboratory variability, and is the subject of a current effort for harmonization.[33] Many labs also add myoepithelial (SMA), epithelial (CK8/18), and lobular differentiation markers (ECAD) to the workup. Recently, a host of new multi-marker panels have been developed and quantitative measures (rather than just positive *vs* negative) have been shown to improve prognostic assessments and predictions of response to therapy. 'IHC4' uses a combined quantitated 'H score' IHC for ER, cell percentages for PR and Ki67, and HER2-staining patterns for prognostic and predictive assessments equal to the best currently available multi-gene molecular assays such as Oncotype DX (Genomic Health, Redwood City, CA, USA).[34] A modification of this assay demonstrated improved predictive power through the addition of the IHC marker, BAG1.[35] The 'Mammostrat' assay (Clarient, Aliso Viejo, CA, USA) uses a panel of five IHC markers (P53, SLC7A5, NRDG1, HTF9C, and CEACAM5).[36] Gene expression (mRNA-based) assays using qRT-PCR, array hybridization, and RNA sequence assays have also been developed. The Oncotype DX assay, eg, uses a panel of 21 genes (16 analytical and 5 controls: Ki67, STK15, Survivin, CCNB1, MYBL2, MMP11, CTSL2, HER2, GRB7, GSTM1, CD68, BAG1, ER, PGR, BCL2, SCUBE2, ACTB, GAPDH, RPLPO, GUS, TFRC) to stratify risk of recurrence and to estimate the relative benefit of adjuvant chemotherapy. This list continues to grow with improved understanding of tumor metabolic phenotypes, and patterns of host stroma and

immune reaction. New multiplexing techniques that combine tyramide-signal amplification and multispectral imaging are being developed and permit complex analyses of the spatial interactions between tumors and many classes of immune cells, eg, see Stack *et al*.[3]

Prostate cancer diagnostics could also benefit from clinically directed multiplexing, as core biopsies could be routinely examined using antibodies defining basal and luminal cells and cells with upregulated racemase,[37,38] as well as antibody panels that might survey protein products of the Genomic Health prostate panel of 17 genes that has been developed to stratify patients into progression-risk categories.[39] It is difficult to get an accurate evaluation of the false-positive and false-negative rates of prostate core biopsies, but it is clear that the use of combined 3-antibody IHC has become much more frequent and has probably decreased these rates. As medical treatments for low-risk prostate cancer become common, biopsy interpretation for atrophy and basal hyperplasia increasingly requires this IHC combination for optimal evaluation. It seems inevitable that interpretation of biopsies from virtually every site will soon depend on specific molecular localizations to support diagnoses with higher sensitivity and specificity, but also for molecular phenotyping to separate diagnoses into actionable prognostic and therapy-predictive categories.

Full appreciation of high-resolution molecular and spatial data that mass-spectrometry-based techniques are generating will require development of new analytical tools. Currently, interpretation of serial-section-based multiplexed IHC data is typically managed using approaches in which each stain is generally defined as either positive or negative: a summary matrix of results is readily generated and interpreted. If, however, graded positivity based on intensity or cell-percentage-positive scores, or both, are added to the mix, the resulting complexity may prevent adoption in the clinic (even when it has been shown provide the same actionable result as more involved gene expression analyses). On the other hand, performing multiplexing on single slides may to some degree reduce the level of complexity encountered, as in contrast to serial-section-based approaches, no spatial co-registration between marker patterns is required. Nevertheless, to be useful in the clinic, simple tools to assist interpretation, such as Boolean-logic-based pseudocoloring (eg, co-expression of one or more analytes), or automated histogram data display similar to that used for flow cytometry will need to be developed.

It is clear, however, that future highly multiplexed studies will outgrow these somewhat familiar tools. More sophisticated, but still purely molecular (non-spatial), approaches to deal with this scale of data currently include the SPADE tools on Cytobank[40] and the ACCENSE method.[41] The former emphasizes hierarchical or developmental connections between cell populations, whereas the latter can detect population clusters without hierarchical constraints. To give an idea of the scale of the challenge: CyTOF data processed through ACCENSE provided cell-by-cell high-dimensional information highlighting the probable existence of at least 24 subclasses of $CD8^+$ T cells.[41] Now, imagine combining such per-cell molecular complexity with geographic distribution tools. These could be used to characterize the spatial distributions of highly refined cell subclasses, and add information on distances and possible interactions between populations, such as immune cell types, and distinct tumor subregions.[42]

Some cautions are in order. The explosion of potentially important or actionable biomarkers poses both cost and logical selection challenges—and there are practical methodological issues that need to be addressed as well. Despite years of work to standardize the three IHC assays in common use in breast cancer workups (ER/PR/HER2), there is still ongoing significant and troubling inter-laboratory and intra-laboratory quantitative variability. If these problems cannot be overcome for these three 'tried-and-true' biomarkers, it is hard to imagine adding 6, 10, not to mention 30+ new markers to the panel with any robustness. The mass-tagged antibody approaches may make this challenge somewhat easier to manage. Thirty tagged antibodies can be incubated simultaneously, reducing the difficulty, time, and therefore cost to perform the multiplex analysis, although, as noted above, pre-analytical variability and details of antigen retrieval methods will need to be very critically explored. Because of the potential sensitivity, low crosstalk and high dynamic range of the metal-labeled antibody approach, many of the difficulties posed by current approaches to multiplexing are minimized.

Is metal-labeled protein (and other analyte) detection really the 'next-gen' step in pathology, as suggested in a recent commentary?[25] We think so. As discussed above, multiple analytical challenges arise when using colorimetric or fluorometric reporters for high-level multiplex IHC analysis. Immunoperoxidase staining intensity is nonlinear and often correlates poorly with antigen concentration. Although IF offers improved dynamic range and signal-to-noise ratios, spectral overlap of reporter emission spectra and the need for primary antibodies generated in dissimilar host species ultimately limit its use in highly multiplexed assays. Although dye-cycling methods can be used to obtain information from many 10's of antibodies, the staining, imaging, destaining process can be technically challenging and time-consuming. The use of metal reporters combined with ion-beam imaging described here is compatible with single-step labeling and imaging, increasing convenience and potential applicability. When it is possible to obtain high-resolution, cell-by-cell, highly multiplexed molecular tumor phenotypes, we anticipate that significant new biological and clinical insights may be gained. For example, spatially resolved evaluation of the activity-state of numerous signaling pathways (eg, via phospho-epitope-sensitive antibodies) in individual cells will be possible. Moreover, the ability to detect multiple molecular species within cells and organelles with ~50-nm

resolution (anticipated)—in 3D—could reveal completely new vistas in basic and translational cell science. Taking advantage of the low, near-zero, signal crosstalk between labels, it is intriguing to consider studies that examine the abundance and functional status of multiple nuclear proteins at once, including less familiar targets such as FGFRR2, NFκB/Rel,[43] EGF, and FGF.[44] In addition, it has not escaped our notice that the methodology we outline here will also permit the multiplexed high-resolution imaging of expressed coding and non-coding RNA molecules.

Can MIBI be made cheap and easy enough to be used routinely? This question depends on a few variables. The actual cost of the primary antibody production will never be as cheap as hematoxylin and eosin, and the instrumentation requirements of SIMS are still prohibitive. Moreover, evaluation of multiple analytes per slide assays will require digital image viewing, with display and analysis tools yet to be optimized for easily transitioning between combinations, and for computer-assisted interpretation. Nevertheless, the incredible value of detailed structure with specific tissue, cellular, and subcellular localization of many different molecular species at once warrants further effort. As outlined above, the instrumentation can be engineered to provide higher throughput and shorter scan times. If single-incubation multiplexed staining cocktails can be deployed for any given clinical scenario, the multiplexing *per se* would have little impact on the workflow. Benefits include a great reduction in the number of physical tissue sections that have to be prepared, stained, imaged, and correlated, and a corresponding improvement in the quality and detail of pathology analysis.

In conclusion, we suggest that metal-labeled probes coupled with high-resolution imaging platforms will provide spatially resolved, multiple molecule detection while overcoming some of the drawbacks of chromogenic or fluorescence detection methods. Metal-labeling approaches offer high sensitivity and dynamic range, stable labeling, little or no channel cross-talk, and potentially even better than conventional optical microscopy resolution. These techniques are compatible with clinical workflow and can be cost-effective. We anticipate that these, along with other highly multiplexed approaches, will yield new insights into basic cell biology, improved understanding of cancer phenotypes, and will have indirect or even direct clinical impact.

ACKNOWLEDGMENTS

This work is funded by the Department of Defense Grant BC132309 –DoD BCRP, NCI IMAT grants 1R21CA183660-01 and 1R33CA183654-01 and funding from the Department of Pathology and Laboratory Medicine, UC Davis.

DISCLOSURE/CONFLICT OF INTEREST

The authors declare no conflict of interest.

1. Simone NL, Bonner RF, Gillespie JW, *et al.* Laser-capture microdissection: opening the microscopic frontier to molecular analysis. Trends Genet 1998;14:272–276.
2. Lubieniecka JM, Nielsen TO. cDNA microarray-based translational research in soft tissue sarcoma. J Surg Oncol 2005;92:267–271.
3. Stack EC, Wang C, Roman KA, *et al.* Multiplexed immunohistochemistry, imaging, and quantitation: A review, with an assessment of Tyramide signal amplification, multispectral imaging and multiplex analysis. Methods 2014;70:46–58.
4. Rimm DL. What brown cannot do for you. Nat Biotechnol 2006;24:914–916.
5. Camp RL, Chung GG, Rimm DL. Automated subcellular localization and quantification of protein expression in tissue microarrays. Nat Med 2002;8:1323–1327.
6. Fountaine TJ, Wincovitch SM, Geho DH, *et al.* Multispectral imaging of clinically relevant cellular targets in tonsil and lymphoid tissue using semiconductor quantum dots. Mod Pathol 2006;19:1181–1191.
7. Bearman GH, Mahadevan-Jansen A, Levenson RM eds) Spectral Imaging: Instrumentation, Applications, and Analysis III, San Jose, CA, 2005.
8. Levenson R, Beechem J, McNamara G. Spectral imaging in preclinical research and clinical pathology. Anal Cell Pathol (Amst) 2012;35:339–361.
9. Tsurui H, Nishimura H, Hattori S, *et al.* Seven-color fluorescence imaging of tissue samples based on Fourier spectroscopy and singular value decomposition. J Histochem Cytochem 2000;48:653–662.
10. Glass G, Papin JA, Mandell JW. SIMPLE: a sequential immunoperoxidase labeling and erasing method. J Histochem Cytochem 2009;57:899–905.
11. Wählby C, Erlandsson F, Bengtsson E, *et al.* Sequential immunofluorescence staining and image analysis for detection of large numbers of antigens in individual cell nuclei. Cytometry B Clin Cytom 2002;47:32–41.
12. Pirici D, Mogoanta L, Kumar-Singh S, *et al.* Antibody elution method for multiple immunohistochemistry on primary antibodies raised in the same species and of the same subtype. J Histochem Cytochem 2009, 57:567–575.
13. Friedenberger M, Bode M, Krusche A, *et al.* Fluorescence detection of protein clusters in individual cells and tissue sections by using toponome imaging system: sample preparation and measuring procedures. Nat Protoc 2007;2:2285–2294.
14. Schubert W, Bonnekoh B, Pommer AJ, *et al.* Analyzing proteome topology and function by automated multidimensional fluorescence microscopy. Nat Biotechnol 2006;24:1270–1278.
15. Schubert W, Gieseler A, Krusche A, *et al.* Toponome mapping in prostate cancer: detection of 2000 cell surface protein clusters in a single tissue section and cell type specific annotation by using a three symbol code. J Proteome Res 2009;8:2696–2707.
16. Zrazhevskiy P, Gao X. Quantum dot imaging platform for single-cell molecular profiling. Nat Commun 2013;4:1619.
17. Clarke GM, Zubovits JT, Shaikh KA, *et al.* A novel, automated technology for multiplex biomarker imaging and application to breast cancer. Histopathology 2014;64:242–255.
18. Zimak J, Schweller RM, Duose DY, *et al.* Programming in Situ Immunofluorescence Intensities through Interchangeable Reactions of Dynamic DNA Complexes. Chembiochem 2012;13:2722–2728.
19. Shcherbatyuk GV, Inman RH, Ghosh S. Anomalous photo-induced spectral changes in CdSe = ZnS quantum dots. J App Phys 2011;110:053518-1-6.
20. Neher R, Neher E. Optimizing imaging parameters for the separation of multiple labels in a fluorescence image. J Microsc 2004;213:46–62.
21. Hollman-Hewgley D, Lazare M, Bordwell A, *et al.* A single slide multiplex assay for the evaluation of classical Hodgkin lymphoma. Am J Surg Pathol 2014;38:1193–1202.
22. Giesen C, Wang HA, Schapiro D, *et al.* Highly multiplexed imaging of tumor tissues with subcellular resolution by mass cytometry. Nat Methods 2014;11:417–422.
23. Angelo M, Bendall SC, Finck R, *et al.* Multiplexed ion beam imaging of human breast tumors. Nat Med 2014;20:436–442.
24. Blow N. Tissue preparation: Tissue issues. Nature 2007;448:959–963.
25. Rimm DL. Next-gen immunohistochemistry. Nat Methods 2014;11:381–383.
26. Senyo SE, Steinhauser ML, Pizzimenti CL, *et al.* Mammalian heart renewal by pre-existing cardiomyocytes. Nature 2013;493:433–436.
27. Zhang D-S, Piazza V, Perrin BJ, *et al.* Multi-isotope imaging mass spectrometry reveals slow protein turnover in hair-cell stereocilia. Nature 2012;481:520–524.

28. Steinhauser ML, Bailey AP, Senyo SE, *et al.* Multi-isotope imaging mass spectrometry quantifies stem cell division and metabolism. Nature 2012;481:516–519.
29. Lechene C, Hillion F, McMahon G, *et al.* High-resolution quantitative imaging of mammalian and bacterial cells using stable isotope mass spectrometry. J Biol 2006;5:20.
30. Williams P. Biological imaging using secondary ions. J Biol 2006; 5:18.
31. Allred DC, Carlson RW, Berry DA, *et al.* NCCN task force report: estrogen receptor and progesterone receptor testing in breast cancer by immunohistochemistry. J Natl Compr Canc Netw 2009;7 (Suppl 6):S1–S21, quiz S2-3.
32. Wolff AC, Hammond ME, Schwartz JN, *et al.* American Society of Clinical Oncology/College of American Pathologists guideline recommendations for human epidermal growth factor receptor 2 testing in breast cancer. J Clin Oncol 2007;25:118–145.
33. Luporsi E, Andre F, Spyratos F, *et al.* Ki-67: level of evidence and methodological considerations for its role in the clinical management of breast cancer: analytical and critical review. Breast Cancer Res Treat 2012;132:895–915.
34. Cuzick J, Dowsett M, Pineda S, *et al.* Prognostic value of a combined estrogen receptor, progesterone receptor, Ki-67, and human epidermal growth factor receptor 2 immunohistochemical score and comparison with the Genomic Health recurrence score in early breast cancer. J Clin Oncol 2011;29:4273–4278.
35. Afentakis M, Dowsett M, Sestak I, *et al.* Immunohistochemical BAG1 expression improves the estimation of residual risk by IHC4 in postmenopausal patients treated with anastrazole or tamoxifen: a TransATAC study. Breast Cancer Res Treat 2013;140:253–262.
36. Bartlett JM, Thomas J, Ross DT, *et al.* Mammostrat as a tool to stratify breast cancer patients at risk of recurrence during endocrine therapy. Breast Cancer Res 2010;12:R47.
37. Sung MT, Jiang Z, Montironi R, *et al.* Alpha-methylacyl-CoA racemase (P504S)/34betaE12/p63 triple cocktail stain in prostatic adenocarcinoma after hormonal therapy. Hum Pathol 2007;38:332–341.
38. Daoud NA, Li G, Evans AJ, *et al.* The value of triple antibody (34betaE12 + p63 + AMACR) cocktail stain in radical prostatectomy specimens with crushed surgical margins. J Clin Pathol 2012;65: 437–440.
39. Klein EA, Cooperberg MR, Magi-Galluzzi C, *et al.* A 17-gene Assay to Predict Prostate Cancer Aggressiveness in the Context of Gleason Grade Heterogeneity, Tumor Multifocality, and Biopsy Undersampling. Eur Urol 2014;66:550–560.
40. Qiu P, Simonds EF, Bendall SC, *et al.* Extracting a cellular hierarchy from high-dimensional cytometry data with SPADE. Nat Biotechnol 2011;29:886–891.
41. Shekhar K, Brodin P, Davis MM, *et al.* Automatic Classification of Cellular Expression by Nonlinear Stochastic Embedding (ACCENSE). Proc Natl Acad Sci USA 2014;111:202–207.
42. Chang AY, Bhattacharya N, Mu J, *et al.* Spatial organization of dendritic cells within tumor draining lymph nodes impacts clinical outcome in breast cancer patients. J Transl Med 2013;11:242.
43. Sovak MA, Bellas RE, Kim DW, *et al.* Aberrant nuclear factor-kappaB/Rel expression and the pathogenesis of breast cancer. J Clin Invest 1997;100:2952–2960.
44. Planque N. Nuclear trafficking of secreted factors and cell-surface receptors: new pathways to regulate cell proliferation and differentiation, and involvement in cancers. Cell Commun Signal 2006;4:7.

Published in final edited form as:
Nat Med. 2014 April ; 20(4): 436–442. doi:10.1038/nm.3488.

Multiplexed ion beam imaging (MIBI) of human breast tumors

Michael Angelo[1,2], **Sean C. Bendall**[1], **Rachel Finck**[1], **Matthew B. Hale**[1], **Chuck Hitzman**[3], **Alexander D. Borowsky**[4], **Richard M. Levenson**[4], **John B. Lowe**[5], **Scot D. Liu**[5], **Shuchun Zhao**[6], **Yasodha Natkunam**[6], and **Garry P. Nolan**[1,†]

[1]Baxter Laboratory in Stem Cell Biology, Department of Microbiology and Immunology, Stanford University, Stanford, CA

[2]Department of Laboratory Medicine, University of California San Francisco, San Francisco, CA

[3]Department of Materials Science and Engineering, Stanford University, Stanford, CA

[4]Department of Pathology and Laboratory Medicine, University of California Davis, Davis, CA

[5]Department of Pathology, Genentech, South San Francisco, CA

[6]Department of Pathology, Stanford University, Stanford, CA

Abstract

Immunohistochemistry (IHC) is a tool for visualizing protein expression employed as part of the diagnostic work-up for the majority of solid tissue malignancies. Existing IHC methods use antibodies tagged with fluorophores or enzyme reporters that generate colored pigments. Because these reporters exhibit spectral and spatial overlap when used simultaneously, multiplexed IHC is not routinely used in clinical settings. We have developed a method that uses secondary ion mass spectrometry to image antibodies tagged with isotopically pure elemental metal reporters. Multiplexed ion beam imaging (MIBI) is capable of analyzing up to 100 targets simultaneously over a five-log dynamic range. Here, we used MIBI to analyze formalin-fixed, paraffin-embedded (FFPE) human breast tumor tissue sections stained with ten labels simultaneously. The resulting data suggest that MIBI will provide new insights by integrating tissue microarchitecture with highly multiplexed protein expression patterns, and will be valuable for basic research, drug discovery and clinical diagnostics.

Introduction

Antibodies were first employed in tissue section analysis in 1942 to visualize pneumococcal antigens in organ biopsies from mice infused with live bacteria[1]. Since that time, immunohistochemistry (IHC) has become a mainstay of clinical diagnostics and basic research and is primarily used to assess the spatial distribution of one or two (rarely more) antigens in tissue sections. Despite the high specificity of many antibodies, the concentration

[†]To whom correspondence can be addressed – gnolan@stanford.edu.

Author Contributions: M.A., S.B., and R.F. conducted experiments and wrote the manuscript. M.H. designed and fabricated reagents. C.H. assisted in data acquisition and experimental design. A.B. and R.L. prepared tissue sections, performed IHC, and assisted in writing the manuscript. J.L., S.L., S.Z., and Y.N. prepared tissue sections, performed IHC, and assisted in optimizing protocols used in MIBI analysis. G.N. assisted in experimental design and wrote the manuscript.

of most antigens is insufficient to permit detection by conventional assays without signal amplification[2-4]. Signal amplification is typically achieved using multivalent, enzyme-linked secondary antibodies that bind the F_c-portion of the primary antibody. In bright-field microscopy, the most commonly used enzymatic reporter is horseradish peroxidase, typically used to oxidize 3,3′-diaminobenzidine (DAB), resulting in accumulation of a brown precipitate. Such non-linear enzymatic amplification can result in poor correlation with the target antigen concentration[2,5].

Simultaneous detection of multiple antigens is subject to additional constraints that limit the utility of existing IHC-based analysis for predictive biomarker development in human clinical trials and clinical diagnostics. Colorimetric detection of four antigens has been reported using multiple enzyme-linked secondary antibodies, but in practice this approach is usually limited to two because of difficulties encountered in sample preparation and imaging[2,6]. Fluorescent labels used in the related immunofluorescence (IF) technique provide a higher signal-to-noise ratio and are more frequently used for simultaneous detection of multiple molecular targets. Practical limitations include the need for primary antibodies generated in dissimilar host species and for non-overlapping reporter emission spectra[5]. Thus, conventional IHC or IF methodologies do not support the robust generation of multiplexed, quantitative data needed to understand the relationship between tissue microarchitecture and expression at a molecular level.

Previous work by our lab, and others, have demonstrated the utility of elemental mass spectrometry in circumventing similar limitations encountered in fluorescence-based flow cytometry[7-11]. In this approach, termed, “mass cytometry”, cells stained with antibodies carrying isotopically pure, non-biological, elemental metal reporters are nebulized into single-cell droplets prior to sequential analysis via inductively-coupled plasma time-of-flight mass spectrometry. In principle, single-cell analysis of up to 100 parameters can be achieved without spectral overlap between channels[11].

Here, we present a modality that uses secondary ion mass spectrometry to image metal isotope carrying antibodies. Multiplexed ion beam imaging (MIBI) is capable of analyzing samples stained simultaneously with up to 100 metal-isotope labeled antibodies and is compatible with standard formalin-fixed, paraffin-embedded (FFPE) tissue sections, the most common type of specimen in clinical repositories worldwide[12]. Depending on the element of interest, MIBI can achieve as low as parts-per-billion sensitivity with a dynamic range of 10^5 and resolution comparable to high-magnification light microscopy[13-16]. We used MIBI to image breast tumor tissue sections stained with clinically relevant metal-conjugated antibodies. The data generated from these experiments could be viewed both in a conventional imaging context as well by using high-dimensional quantitative immunophenotypic feature analysis compatible with higher levels of multiplexing and that can allow classification and unsupervised analysis of each biopsy.

Results

Performance assessment of MIBI

The workflow for MIBI is comparable to IF and IHC assays (Fig. 1). Instead of fluorophores or enzyme-conjugated reagents, biological specimens are incubated with primary antibodies coupled to stable lanthanides highly enriched for a single isotope (Fig. 1). Primary antibodies are combined in solution for simultaneous incubation with the specimen. The specimens prepared for MIBI are mounted in a sample holder and subjected to a rasterized oxygen duoplasmatron primary ion beam. As this ion beam strikes the sample lanthanide adducts of the bound antibodies are liberated as secondary ions. In this study, the secondary ions are subsequently analyzed via a magnetic sector mass spectrometer equipped with multiple detectors, permitting parallel detection of multiple lanthanide isotopes (mass-based reporters). The resultant data produces a two-dimensional map of the elemental distribution of each lanthanide, and thus each antibody and its corresponding epitope.

As part of preliminary validation studies, peripheral blood mononuclear cells (PBMC) stained with seven metal isotope-conjugated primary antibodies (CD3, CD4, CD8, CD14, CD19, CD45, HLA-DR) were assessed in parallel using mass cytometry and MIBI (Fig. 2). Mass cytometry was performed on the PBMC suspension as described previously[7]. For MIBI, cells were immobilized on a poly-l-lysine-coated silicon wafer, dried under vacuum, and subsequently analyzed using a NanoSIMS 50L™ mass spectrometer. Sequential 50-μm fields were each scanned for 5 min (Fig. 2a). 10-μm overlapping regions of each field were aligned to construct a composite mosaic using an automated script in Matlab. The resultant mosaic was segmented into single-cell regions of interest (ROIs) using the CD45 channel[17]. To extract single cell expression data for each antibody, the ion count for each channel was integrated for each cell ROI. To achieve this mosaic, 1190 fields were imaged for 5 min per field (99 h total scan time). However, as discussed below, orders-of-magnitude improvements in throughput can be achieved with appropriate sample preparation and instrumentation modifications.

Mass cytometry and MIBI produced comparable results and qualitative patterns of expression when analyzed via traditional biaxial plots (Fig. 2b) with marker intensities determined by MIBI demonstrating a dynamic range of 10^5. Additionally, both platforms yielded quantitatively similar frequencies for seven manually gated cell populations (Fig. 2c), with three of these populations differing by less than 1% between platforms (B-cells, $CD8^+$ T-cells, $CD4^+$ T-cells). Altogether, using PBMCs as a test case, MIBI yielded both qualitatively and quantitatively equivalent results as a conventional analytical platform while also revealing spatial features of protein expression at the subcellular level.

Ten color imaging of human breast tumor tissue sections

In order to utilize MIBI for analysis of tissue sections acquired in a diagnostic setting, we sought to verify the performance of metal-conjugated versions of the antibodies used in conventional IHC staining by comparing staining behavior of metal-conjugated vs. unmodified primary antibodies. Secondary staining of serial sections from a single FFPE human breast tumor tissue block treated with metal-conjugated or unmodified primary

antibodies for Ki67 or estrogen receptor alpha (ER) demonstrate positive nuclear staining of comparable intensity and similar levels of background staining (Fig. 3a), indicating that the metal conjugation did not materially affect specific and non-specific staining behavior.

Finally, to assess the overall performance of MIBI in a diagnostic imaging application FFPE breast tumor tissue sections from three different patients with different immunophenotypic profiles were analyzed. ER, progesterone receptor (PR), and HER2 positivity were verified in a clinical IHC lab using validated reagents. For MIBI, tumor sections were mounted on poly-l-lysine-coated silicon wafers, deparaffinized, and subjected to heat-induced epitope retrieval prior to overnight staining with metal-conjugated antibodies for dsDNA, ER, progesterone receptor (PR), e-cadherin, Ki67, vimentin, actin, keratin, and HER2. Conveniently, a hematoxylin counterstain can be readily detected by measuring its elemental aluminum content. The following day the sections were washed, counterstained with hematoxylin, and dehydrated via graded ethanol series.

Using the MIBI analysis, conventional high-resolution images can be generated using FFPE tissues. Ten marker images were acquired in two consecutive scans of the same 80-μm field of view, each scan lasting 25 min. Hematoxylin, ER, PR, Ki67, e-cadherin, her2, and dsDNA were acquired during the first scan, and keratin, vimentin, and actin during the second. Pseudo-brightfield images mimicking traditional DAB staining were constructed by encoding hematoxylin on a white-to-blue scale while putting the desired marker on a white to brown scale (Fig. 3b, **top**). Pseudo-fluorescence images mimicking three-color immunofluorescence were constructed using a red-encoded dsDNA channel, a blue-encoded hematoxylin channel, and a green encoded marker channel (Fig. 3b, **bottom**). Pseudo-brightfield and pseudo-fluorescence composites for each antibody within a single field of view are shown for each of the three tissue sections (Fig. 3c). Comparison of HER2-, ER-, and PR-positivity across the three specimens demonstrates appropriate expression with respect to immunophenotypes established by conventional IHC staining. Sections expressing ER and PR demonstrate well-demarcated nuclear staining, scattered Ki67-positive nuclei, and intense positive staining for vimentin in mesenchymal cells. $HER2^+$ sections demonstrate strong membrane staining. E-cadherin, actin, and keratin also demonstrate appropriate subcellular staining patterns.

Image segmentation and feature extraction

In order to further explore the utility of the information inherent in the quantitatively multiplexed images in this study, image segmentation was performed so that cellular features could be analyzed and compared. Hematoxylin and dsDNA channels for each tumor were segmented using CellProfiler in order to extract summary statistics describing subcellular expression[18,19] (Fig. 4a). The pixel intensity for each marker and subcellular ROI demonstrate distinctly different distributions with respect to the known immunophenotype of each tumor (Supplementary Fig. S1). Mean pixel intensities were quantified for each marker within nuclear, cytoplasmic, and cellular ROIs for each cell. Biaxial scatter plots demonstrate marker coexpression matching the known immunophenotype for each tumor (Fig. 4b). Triple-positive and ER^+PR^+ tumors demonstrate appropriate nuclear co-expression of ER and PR that is absent in the

$HER2^{+}ER^{-}PR^{-}$ tumor. Subpopulations of keratin, e-cadherin-positive ductal cells are distinctly segregated from vimentin-positive mesenchymal cells.

Quantitative accuracy was further assessed by comparing MIBI to an FDA-approved quantitative image analysis (QIA) workflow for determining the staining intensity of scanned IHC tissue sections. QIA was used to quantify ER nuclear expression in a cohort of breast tumors. Tumor-containing regions were manually annotated and subsequently analyzed using an automated algorithm optimized for determining immunoperoxidase nuclear staining intensity. The resultant data included mean intensity, as well as an overall H-score. Linear regression analysis comparing mean ER nuclear staining intensity by MIBI or IHC demonstrated robust agreement between the two methods (Fig. 4c **top**, $r = 0.99$, $P < 0.00001$). Cutoffs for MIBI staining intensity were calculated with the resultant linear equation ($MIBI = 0.064 + 0.0073*IHC$) using the respective values for negative, 1+, 2+, and 3+ employed by QIA and subsequently used to calculate an overall H-score. Linear regression analysis comparing IHC and MIBI H-scores also demonstrate strong, robust agreement (Fig. 4c bottom, $r = 0.99$, $P < 0.00001$) with a slope near unity ($m = 1.06 \pm 0.06$SD). The strong correlation between H-scores derived using the two methods suggests that MIBI not only captured the mean overall staining intensity, but also was able to accurately capture the biological variability of ER expression. This implies that the true distribution of staining intensity was valid and accurately recapitulated. These results also suggest that, at least within the context of its application here, MIBI analysis is not materially affected by sample-to-sample matrix effects that can arise when using a bioanalysis platform. Furthermore, comparison of ER staining intensity in serial sections treated with either all nine antibodies or ER only show that the quantitative accuracy of this method is unaffected by multiplexing (Supplementary Fig. S2).

Integrated histological and immunophenotypic features of multidimensional MIBI data can be visualized by generating composite images that combine quantitative (continuous) cytoplasmic and categorical (positive or negative) nuclear expression patterns (Fig. 5). Hormone-receptor-positive regions within the epithelial compartment, showing variable non-nuclear expression of actin (*red*) and e-cadherin (*green*), can be distinguished from interspersed mesenchymal cells co-expressing actin (red) and vimentin (*blue*). Approximately 8% of cells are seen to be $Ki67^{+}$. Unlike conventional chromogenic IHC, which is not well-suited to detecting co-localization of multiple markers, MIBI analysis readily demonstrates $ER^{+}PR^{+}$ (*aqua*) or $ER^{+}PR^{+}Ki67^{+}$ (*yellow*) subpopulations.

Discussion

In this study, we have presented and validated elemental-mass-based multiplexed IHC analysis that circumvents the limitations associated with conventional staining methods relying on optical absorbance or fluorescence signals. This method can be used on virtually any vacuum-compatible specimen, including FFPE tissue. FFPE tissue is the most common type of specimen, with an estimated 1 billion blocks stored in clinical repositories globally[11]. In validating this method we were able to demonstrate an almost quantitatively identical immunophenotypic analysis of PBMCs compared to a more conventional approach (Fig. 2) as well as equivalent (staining pattern and intensity) imaging of FFPE breast tumors

with different immunophenotypes with the additional benefit of simultaneous staining of ten or more markers (Fig. 3). Additionally, marker multiplexing and image segmentation permitted quantitative feature extraction describing cellular and subcellular expression, that in aggregate, revealed immunophenotypes of cell subpopulations that could be related back to the original clinical pathology of the tissue (Fig. 4). The quantitative accuracy of MIBI was demonstrated via side-by-side comparison with an FDA-approved QIA IHC platform. Finally, novel approaches in combinatorial false (or pseudo-) coloring of images could distill the high-dimensional analysis down to a rapidly interpretable single image in which multiple phenotypes could be represented by single colors in an automated fashion (Fig. 5).

MIBI has a number of advantages over conventional IHC techniques. Background signal due to autofluorescence is absent and the dynamic range presented here is already 10^5, exceeding immunofluorescence and chromogenic IHC by 100-fold and 1000-fold, respectively[2,20,21]. Because the mass accuracy can resolve less than a fraction of a Dalton at even the lowest resolution (Supplementary Fig. S3) no spectral overlap is observed between mass adjacent elemental reporters. Moreover, the reporter panel can be designed such that neither the residual isotopic contaminants (Supplementary Fig. S3 and Supplementary Table S1) nor the metal oxide abducts (Supplementary Figs. S4 and S5) interfere materially with the reporter masses associated with each antibody probe, obviating the need for channel compensation in the experiments herein. Assay linearity is improved relative to both chromogenic IHC and IF because neither secondary labeling nor amplified detection are required[2]. Meanwhile, relatively conventional methods are used for immunoreactions, and because mass tags do not degrade, samples are stable indefinitely, permitting remote preparation together with a centralized reading facility.

Immunofluorescence-based high-level multiplexing assays have been reported previously. Multispectral imaging with careful selection of antibodies, secondary antibodies, fluorescent dyes and filter cubes can be used to achieve multiplexing up to seven simultaneous labels, although such performance is rarely achieved, and requires much optimization[22]. Sequential methods for multiplexing, sometimes referred to as “dye cycling”, have been described that use the general approach of repeated cycles of primary staining (with or without secondary staining), imaging, and then quenching or bleaching or otherwise removing each cycle's fluorescent reporters. Methods for erasing the signals have included low-pH antibody elutions, high-temperature fluorophore denaturation, antibody stripping, or photobleaching[23-28]. These approaches have several shortcomings not found with MIBI. Some methods of dye cycling lead to accumulative structural changes that alter epitope antigenicity[23]. The techniques typically use just a few primary antibodies per round of staining, making the iterative methodology labor-intensive and time-consuming. Repeated processing of tissue sections can lead to altered histology that reduces the accuracy of image co-registration across staining cycles. In contrast, samples prepared for MIBI are stained with all antibodies in a single step. Markers are acquired in parallel in a single imaging session without any additional sample processing. Furthermore, histological stains, such as hematoxylin, are also detectable with this technique and can be overlaid with antibody expression data making the representations created here indistinguishable from conventional IHC-based pathological analyses.

Other mass-based reporter systems have been used to image FFPE tissues before[29]. These have taken two forms: 1) matrix-assisted laser desorption ionization (MALDI) MS, and 2) laser-ablation (LA) inductively coupled plasma (ICP) MS. MALDI-MS imaging, while adept at analyzing macromolecules, has inherent limitations due to its requirement for a crystalline chemical matrix[30-32]. The matrix combined with the instrument sensitivity reduces achievable resolution (>5 μm) and obscures the signal from elemental reporters. LA-ICP-MS imaging, on the other hand, offers many of the same benefits as MIBI (dynamic range, multiplexing of isotopic reporters). However, laser spot size and instrument sensitivity in previous studies have been limited in elemental reporter-based imaging assays. As such, imaging studies of FFPE breast carcinoma using commercially available LA-ICP-MS systems have yielded images with around 100-μm resolution[33]– a factor of 10^3 less than the MIBI analysis presented here. Altogether, such practical constraints would limit the wide application of previously reported mass-based techniques in a clinical setting as compared to MIBI.

One obstacle to broader application of this method is sample throughput. For antigens expressed at levels similar to those analyzed here, a 100-μm field of view for seven antibodies at a resolution comparable to light microscopy (200–300 nm) can be acquired in as little as 5 min. At this rate, 500-μm field of view would require approximately 2 h to image. Larger numbers of antibodies could be acquired with repeat scans, though this would increase the scan time proportionally, however. In future work, we expect to ameliorate the majority of these issues by employing newly developed primary ion beam sources as well as new instrument configurations. Next-generation oxygen ion sources with higher current densities and 50-nm beam spot sizes have recently become commercially available theoretically permitting ∼20-fold faster image acquisition than the current implementation described here[34]. This new ion beam source will provide lateral resolution comparable to confocal microscopy and axial resolution that exceeds it[34]. Furthermore, new instrument configurations utilizing a time-of-flight (TOF) mass analyzer would permit parallel quantification of all mass reporters in a given experiment without a cyclic analysis. Taken together, gains from these achievable next-generation instrument configurations should reduce the duty cycle for 50–100 targets (mass reporters) in a 500 μm field of view to 5–10 min when imaged at resolutions equal to light microscopy.

In addition to instrument improvements, lanthanide metal antibody conjugation protocols achieve labeling efficiencies of 100–200 metal atoms per antibody[8]. The development of new nanoparticle-based reagents are projected to enable the attachment of up to 10,000 metal atoms per antibody. Such gains in labeling efficiency could further reduce scan times by as much as two orders of magnitude, such that a tumor microarray containing 1,000 600 μm core specimens could be imaged in as little as 1.5 h.

As a consequence of using antibodies for protein detection, MIBI inherits many of the issues that can limit the utility of conventional IHC. Poorly characterized reagents can exhibit non-specific binding, and some epitopes are difficult to target with antibody-based approaches. However, we expect that reagents can be developed which extends the capability of MIBI to other arenas and away from antibody-based analysis, such as *in situ* hybridization and subcellular metabolic analysis. The extended applications of MIBI taken with the gains

permitted by relatively minor modifications of existing analytical systems introduce the prospect of a practical, multiplexed imaging platform that integrates tissue histology, protein expression, gene expression, and metabolism on a subcellular level. The basic science utility of such a system is evident, and clinical deployment of this technology would extend multiplexed expression analysis typically restricted to flow cytometry of cell suspensions (such as blood) to any solid tissue. Given the transformative effect that flow cytometry has shown in the diagnosis, staging, and treatment of hematopoietic malignancies, the present approach, applied to solid tissue samples could provide new insight into disease pathogenesis, address pathway activation status, explore tumor heterogeneity, document effects of therapeutic interventions, and, it is to be hoped, improve patient outcomes.

Online Methods

Substrate preparation

Silicon wafers (Silicon Valley Microelectronics) were diced into 18mm^2 pieces, rinsed two times with methanol, and polished with a cotton-tipped applicator. Cleaned substrates were subsequently immersed in 2% poly-l-lysine solution (Sigma-Aldrich) for 10 min and baked at 60 °C for 1 hr.

Antibodies

A summary of antibodies, reporter isotopes, and concentrations can be found in Table S1 and S2. Metal conjugated primary antibodies were prepared 100 μg at a time using the MaxPAR antibody conjugation kit (DVS Sciences, Toronto, Canada) according to the manufacturer's recommended protocol. Following labeling, antibodies were diluted in Candor PBS Antibody Stabilization solution (Candor Bioscience GmbH, Wangen, Germany) to 0.4 mg mL^{-1} and stored long-term at 4 °C.

Cells

Unmatched human peripheral blood was purchased from the Stanford Blood Bank according to an IRB-approved protocol. All blood samples were collected in heparin sulfate anticoagulant, stored at room temperature for 4–6 hrs, and then separated over Ficoll-Paque Plus (Amersham Biosciences) using Accuspin tubes (Sigma-Aldrich, St. Louis, MO) to remove erythrocytes, platelets, and granulocytes. Cells were frozen in FCS with 10% DMSO. Cells were rested at 37 °C, 5% CO_2 for 1 h in RPMI with 10% FCS (supplemented with 2mM EDTA in the case of frozen samples), 1X L-glutamine and 1X penicillin with streptomycin (Invitrogen).

Staining of peripheral blood mononuclear cells

Cellular staining protocols were based on procedures previously described. Briefly, after resting cells for 1 hr, surface marker antibodies were added yielding 100 μL final reaction volumes and incubated at room temperature for 30 min. Following incubation, cells were washed two times with cell staining media and split into two aliquots. For mass cytometry analysis, cells were permeabilized with 4 °C methanol for 10 min at 4 °C, washed twice with cell staining media to remove residual methanol, and then stained with 1 mL of 1:4000 ^{191,193}Ir DNA intercalator diluted in PBS with 1.6% PFA for 20 min at room

temperature. Cells were then washed once with cell staining media, once with PBS, and then diluted in dH_2O to approximately 10^6 cells mL^{-1} prior to analysis. For MIBI analysis, 50 μL of cells diluted in PBS to approximately 10^7 cells mL^{-1} were placed on silicon substrate and allowed to adhere for 20 min. The substrate was then gently rinsed with PBS, fixed for 5 min in PBS with 2% glutaraldehyde, and rinsed twice with dH_2O. Lastly, samples were dehydrated via a graded ethanol series, air dried at room temperature, and stored in a vacuum desiccator for at least 24 hrs prior to analysis.

Breast tumor tissue sections

Tissue sections (4 μm thickness) were cut from FFPE tissue blocks of human breast tumor using a microtome, mounted on poly-l-lysine-coated silicon substrate for MIBI analysis or a glass slide for immunoperoxidase (IPOX) staining. Silicon-mounted sections were baked at 65 °C for 15 min, deparaffinized in xylene, and rehydrated via a graded ethanol series. The sections were then immersed in epitope retrieval buffer (10 mM sodium citrate, pH 6) and placed in a pressure cooker for 30 min (Electron Microscopy Sciences, Hatfield, PA). The sections were subsequently rinsed twice with dH_2O and once with wash buffer (TBS, 0.1% Tween, pH 7.2). Residual buffer was removed by gently touching the surface with a lint-free tissue prior to incubating with blocking buffer for 30 min (TBS, 0.1% Tween, 3% BSA, 10% donkey serum, pH 7.2). Blocking buffer was subsequently removed and the sections were stained overnight at 4 °C in a humidified chamber. The following morning, the sections were rinsed twice in wash buffer, postfixed for 5 min (PBS, 2% glutaraldehyde), rinsed in dH_2O, and stained with Harris hematoxylin for 10s. Finally, the sections were dehydrated via graded ethanol series, air dried at room temperature, and then stored in a vacuum desiccator for at least 24 hrs prior to imaging. Antigen retrieval was performed using a Decloaking Chamber (Biocare Medical, Concord, CA) with citrate buffer at pH 6.0, 125 °C and pressure to 15 psi. The total time slides were in the chamber was 45 min. Incubations with primary antibodies were performed at room temperature overnight in a humidified chamber. Normal goat serum was used for blocking. Biotinylated goat anti-rabbit (1:1000) was the secondary antibody used with a Vectastain ABC Kit Elite and a Peroxidase Substrate Kit DAB (Vector Labs, Burlingame, CA) used for amplification and visualization of signal, respectively. Tissues known to contain each assessed antigen were used as positive controls.

MIBI analysis

MIBI analysis was performed with a NanoSIMS 50L mass spectrometer (Cameca) using an O^- primary ion beam supplied by an oxygen duoplasmatron source. The primary optics, secondary optics, and mass spectrometer were tuned prior to each experiment. The seven detector trolleys were tuned to the elemental peak corresponding to each metal isotope conjugated antibody using antibody master mixes that had been air dried on silicon. Images containing more than seven channels were acquired by recalibrating the detector trolleys between repeat scans of the same field. The detectors were tuned to the following masses for the first imaging cycle: detector 1 – 27Al, detector 2 – 139La, detector 3 – 143Nd, detector 4 – 147Sm, detector 5 – 158Gd, detector 6 – 166Er, detector 7 – 176Yb. The following settings were used for the second imaging cycle: detector 4 – 154Sm, detector 5 – 162Dy, detector 6 – 168Er. All data were taken in positive ion mode using D1 aperture 2, D0

aperture 0 or 3, and L1 voltage of approximately 1500 V. Because resolving the metal isotopes of interest requires only unit resolution, entrance slit 0 and aperture slit 0 were used in order to maximize ion transmission to the detectors (Fig. S1 and S2). ROIs identified on serial sections using brightfield microscopy were located using the CCD camera in the NanoSIMS analysis chamber. Ion images were acquired over a 50–100 μm fields of view with pixel dwell times between 2–10 ms and up to 10 repeat scans over a single area. Total scan time for a single field of view ranged between 5–25 min. Larger areas were constructed by stitching together multiple contiguous fields of view into a single mosaic.

Mass cytometry measurement

Cell events were collected on a CyTOF mass cytometer as previously described[6]. With detection in dual counting mode using the 'data' calibration, cell length was set to range from 10–75 with a convolution threshold of 100. A detector stability delay of 20 s was used and all samples were diluted such that the acquisition rate was less than 500 cells per second.

PBMC mosaic stitching

The MIBI PBMC data was collected in a series of 1200 individual square 50 μm (128 pixel) tiles, arranged in a 40x30 rectangle. The relative positions of the tiles were determined using the log-transformed CD45 images. The reported offset between adjacent tiles was 40 μm in both the x- and y-directions, but the actual offset was observed to vary due to imprecision in the stage's location. To account for this, each tile was initially placed according to its reported offset, and then moved around 1–20 pixels in both the x- and y-directions to multiple different positions. At each location, the correlation in the overlap area between the new tile and previous tile was computed. The tile was then assigned to the position that maximized the correlation of the overlapped areas.

PBMC image segmentation

The log-transformed mosaic of CD45 tiles was convolved with a 2-dimensional Gaussian kernel with standard deviation of 3 pixels, and then thresholded at a density of 1. Each continuous region with density greater than this threshold was preliminarily labeled as an individual cell. The next step was to separate into their constituent singlets any sets of multiple cells that were close enough to be initially labeled as single cells. To do this, for each preliminary cell, the two points on the boundary were identified between which there was the maximum ratio of distance along the boundary to Euclidean distance (the "pinch points"). When this ratio exceeded 0.42 (a heuristic cutoff), the preliminary cell was separated into two cells with a new border segment between the pinch points. This process was iterated over all cells, and repeated with each new preliminary cell created, until no cells had pinch points that exceeded this separation criteria[17].

Once the cell boundaries were determined, the raw values of each channel measured were summed within each boundary to create a table of total ion intensity on a per-cell basis. The number of pixels within each cell was also calculated as a measure of cell size. This table was equivalent to an .fcs file such as from a standard mass cytometry experiment.

Data analysis

To filter out doublets and debris, singlets were gated from the mass cytometry PBMCs by applying standard cell-length by DNA and then cell-length by CD45 gates; a singlet gate using cell area by CD45 was applied to the MIBI PBMCs. The subsequent gating scheme for both the MIBI and CyTOF processed PBMCs is shown in Figs. 2a and c, respectively.

Supplementary Material

Refer to Web version on PubMed Central for supplementary material.

Acknowledgments

We thank Neil Hubbard, Carmina Espiritu, Sandra Rost, Linda Rangell, and the Genentech Human Tissue labs for assistance in preparing and processing tissue sections. We also thank Astraea Jager for technical support with the CyTOF and antibody labeling. M.A. is supported by the Stanford Molecular Imaging Scholars program through the US National Institutes of Health (NIH 5R25CA11868107). S.C.B. is supported by the Damon Runyon Cancer Research Foundation Fellowship (DRG-2017-09) and US National Institutes of Health (1K99 GM104148-01). This work was supported by grants from the US National Science Foundation (0922648), the US National Institutes of Health (0158 G KB065, 1R01CA130826, 5U54CA143907, HHSN272200700038C, N01-HV-00242, 41000411217, 5-24927, P01 CA034233-22A1, P01 CA034233-22A1, PN2EY018228, RFA CA 09-009, RFA CA 09-011, U19 AI057229, U54CA149145), the California Institute for Regenerative Medicine (DR1-01477, RB2-01592), the European Commission (HEALTH.2010.1.2-1), the US Food and Drug Administration (HHSF223201210194C: BAA-12-00118), and the US Department of Defense (W81XWH-12-1-0591 OCRP-TIA NWC).

References

1. Coons AH, Creech HJ, Jones RN, Berliner E. The demonstration of pneumococcal antigen in tissues by the use of fluorescent antibody. J Immunol. 1942; 45:159–170.
2. Rimm DL. What brown cannot do for you. Nat Biotechnol. 2006; 24:914–916. [PubMed: 16900128]
3. Anagnostou VK, et al. Analytic variability in immunohistochemistry biomarker studies. Cancer Epidemiol Biomarkers Prev. 2010; 19:982–991. [PubMed: 20332259]
4. Bordeaux J, et al. Antibody validation. BioTechniques. 2010; 48:197–209. [PubMed: 20359301]
5. McCabe A, Dolled-Filhart M, Camp RL, Rimm DL. Automated quantitative analysis (AQUA) of in situ protein expression, antibody concentration, and prognosis. J Natl Cancer Inst. 2005; 97:1808–1815. [PubMed: 16368942]
6. Hasui K, et al. Double autoimmunostaining with glycine treatment. J Histochem Cytochem. 2003; 51:1169–1176. [PubMed: 12923242]
7. Bendall SC, et al. Single-cell mass cytometry of differential immune and drug responses across a human hematopoietic continuum. Science. 2011; 332:687–696. [PubMed: 21551058]
8. Lou X, et al. Polymer-based elemental tags for sensitive bioassays. Angew Chem Int Ed Engl. 2007; 46:6111–6114. [PubMed: 17533637]
9. Ornatsky OI, et al. Development of analytical methods for multiplex bio-assay with inductively coupled plasma mass spectrometry. J Anal Atom Spectrom. 2008; 23:463–469.
10. Ornatsky O, et al. Highly multiparametric analysis by mass cytometry. J Immunol Methods. 2010; 361:1–20. [PubMed: 20655312]
11. Bandura DR, et al. Mass cytometry: technique for real time single cell multitarget immunoassay based on inductively coupled plasma time-of-flight mass spectrometry. Anal Chem. 2009; 81:6813–6822. [PubMed: 19601617]
12. Blow N. Tissue preparation: Tissue issues. Nature. 2007; 448:959–963. [PubMed: 17713539]
13. Lechene C, et al. High-resolution quantitative imaging of mammalian and bacterial cells using stable isotope mass spectrometry. J Biol. 2006; 5:20. [PubMed: 17010211]

14. Senyo SE, et al. Mammalian heart renewal by pre-existing cardiomyocytes. Nature. 2013; 493:433–436. [PubMed: 23222518]
15. Steinhauser ML, et al. Multi-isotope imaging mass spectrometry quantifies stem cell division and metabolism. Nature. 2012; 481:516–519. [PubMed: 22246326]
16. Williams P. Biological imaging using secondary ions. J Biol. 2006; 5:18. [PubMed: 17029649]
17. Gordon A, et al. Single-cell quantification of molecules and rates using open-source microscope-based cytometry. Nat Meth. 2007; 4:175–181.
18. Carpenter AE, et al. CellProfiler: image analysis software for identifying and quantifying cell phenotypes. Genome Biol. 2006; 7:R100. [PubMed: 17076895]
19. Kamentsky L, et al. Improved structure, function and compatibility for CellProfiler: modular high-throughput image analysis software. Bioinformatics. 2011; 27:1179–1180. [PubMed: 21349861]
20. Bodo J, Durkin L, Hsi ED. Quantitative In Situ Detection of Phosphoproteins in Fixed Tissues Using Quantum Dot Technology. J Histochem Cytochem. 2009; 57:701–708. [PubMed: 19332430]
21. Camp RL, Chung GG, Rimm DL. Automated subcellular localization and quantification of protein expression in tissue microarrays. Nat Med. 2002; 8:1323–1327. [PubMed: 12389040]
22. Tsurui H, et al. Seven-color fluorescence imaging of tissue samples based on Fourier spectroscopy and singular value decomposition. J Histochem Cytochem. 2000; 48:653–662. [PubMed: 10769049]
23. Glass G, Papin JA, Mandell JW. SIMPLE: a sequential immunoperoxidase labeling and erasing method. J Histochem Cytochem. 2009; 57:899–905. [PubMed: 19365090]
24. Wählby C, Erlandsson F, Bengtsson E, Zetterberg A. Sequential immunofluorescence staining and image analysis for detection of large numbers of antigens in individual cell nuclei. Cytometry. 2002; 47:32–41. [PubMed: 11774347]
25. Pirici D, et al. Antibody elution method for multiple immunohistochemistry on primary antibodies raised in the same species and of the same subtype. J Histochem Cytochem. 2009; 57:567–575. [PubMed: 19223296]
26. Friedenberger M, Bode M, Krusche A, Schubert W. Fluorescence detection of protein clusters in individual cells and tissue sections by using toponome imaging system: sample preparation and measuring procedures. Nat Protoc. 2007; 2:2285–2294. [PubMed: 17853885]
27. Schubert W, et al. Analyzing proteome topology and function by automated multidimensional fluorescence microscopy. Nat Biotechnol. 2006; 24:1270–1278. [PubMed: 17013374]
28. Schubert W, Gieseler A, Krusche A, Hillert R. Toponome mapping in prostate cancer: detection of 2000 cell surface protein clusters in a single tissue section and cell type specific annotation by using a three symbol code. J Proteome Res. 2009; 8:2696–2707. [PubMed: 19275201]
29. Wu B, Becker JS. Imaging of elements and molecules in biological tissues and cells in the low-micrometer and nanometer range. Int J Mass Spectrom. 2011; 307:112–122.
30. Seeley EH, Caprioli RM. Imaging mass spectrometry: Towards clinical diagnostics. Proteomics Clin Appl. 2008; 2:1435–1443. [PubMed: 21136792]
31. Aerni HR, Cornett DS, Caprioli RM. High-throughput profiling of formalin-fixed paraffin-embedded tissue using parallel electrophoresis and matrix-assisted laser desorption ionization mass spectrometry. Anal Chem. 2009; 81:7490–7495. [PubMed: 19650658]
32. Caprioli RM. Perspectives on imaging mass spectrometry in biology and medicine. Proteomics. 2008; 8:3679–3680. [PubMed: 18780396]
33. Giesen C, et al. Multiplexed Immunohistochemical Detection of Tumor Markers in Breast Cancer Tissue Using Laser Ablation Inductively Coupled Plasma Mass Spectrometry. Anal Chem. 2011; 83:8177–8183. [PubMed: 21923169]
34. Smith NS, Tesch PP, Martin NP, Kinion DE. A high brightness source for nano-probe secondary ion mass spectrometry. Appl Surf Sci. 2008; 255:1606–1609.

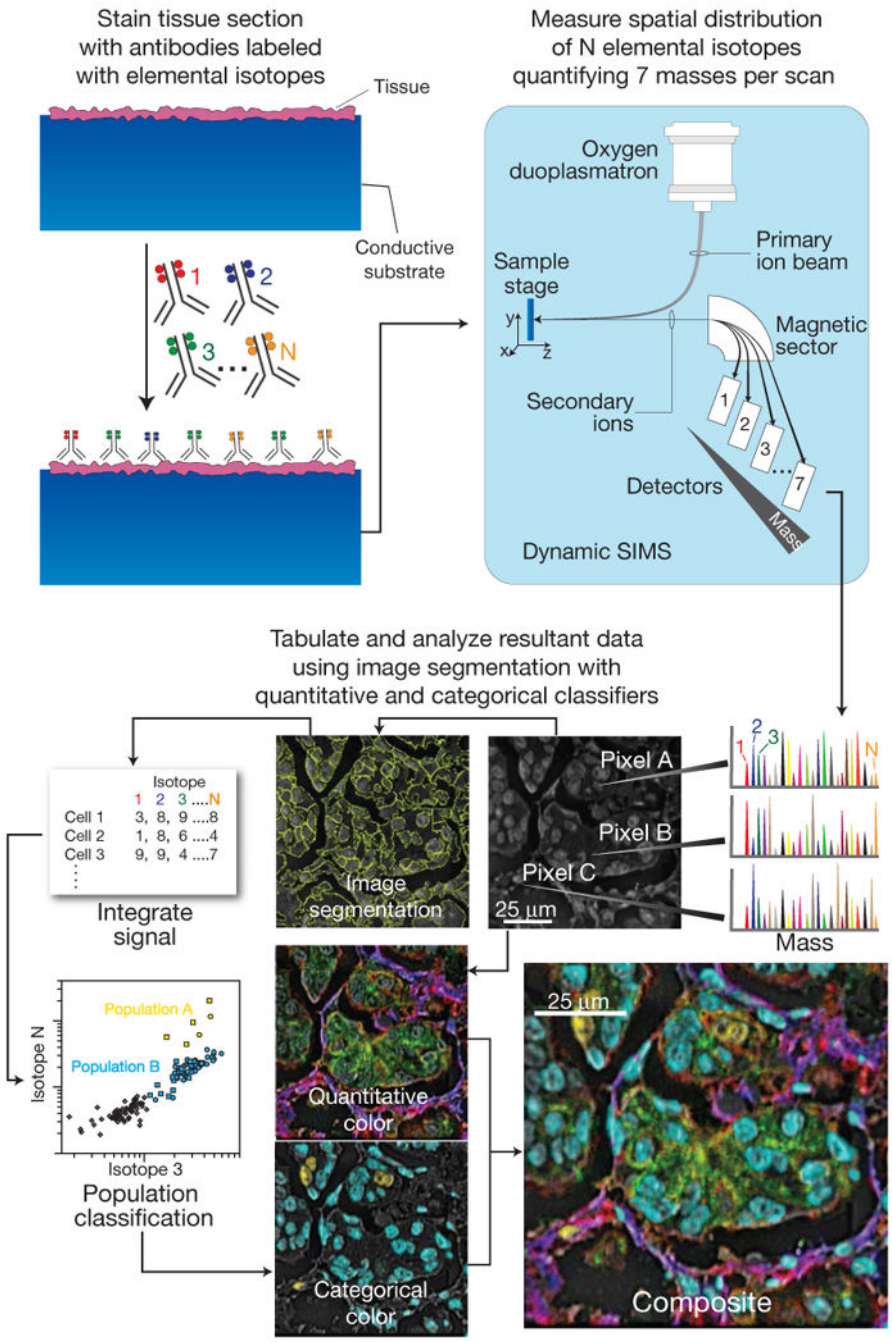

Figure 1. Workflow summary of multiplexed ion beam imaging (MIBI)

Biological specimens, such as FFPE tissue or cell suspensions, are immobilized on a conductive substrate, such as indium tin oxide coated glass or silicon wafer. Samples are subsequently stained with antibodies conjugated to unique transition element isotope reporters, dried, and loaded under vacuum for MIBI analysis. The sample surface is rasterized with a primary ion beam (O^-) that sputters the antibody-specific isotope reporters native to the sample surface as secondary ions. Metal conjugated antibodies are quantified via replicate scans of the same field of view, where up to seven metals reporters are

measured with each scan, and the detectors are mass calibrated in between each scan cycle. Regions of interest demarcating nuclear and cytosolic compartments of each cell are integrated, tabulated, and categorized. Composite images comprised of pseudo-colored categorical features and quantitative three-color overlays are constructed to summarize multidimensional expression data.

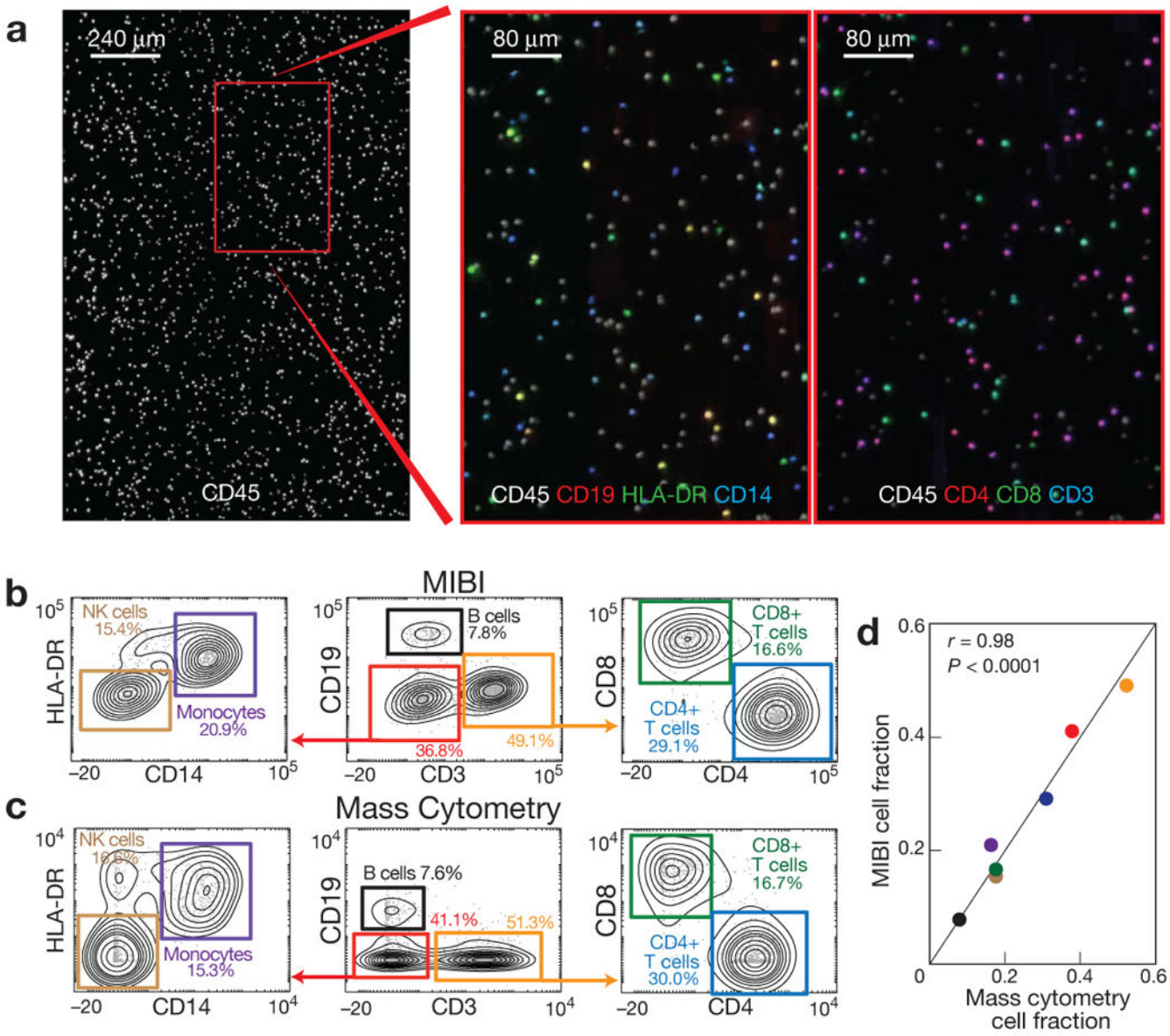

Figure 2. Analysis of PBMCs stained with metal-conjugated antibodies using mass cytometry and MIBI

(**a**) PBMCs stained with seven antibodies were immobilized on a silicon wafer and imaged using MIBI. Single cell regions of interest were segmented using CD45 surface expression and integrated for each antibody. (**b, c**) Hierarchical gating of the resultant data yielded comparable values for seven cell populations relative to those found by mass cytometry. Biaxial plots are arcsinh(x/5) scaled. (**d**) Pearson correlation of the relative abundance of each cell population demonstrated strong agreement between the two methods ($r = 0.98$, $P < 0.0001$, two-tailed t-test).

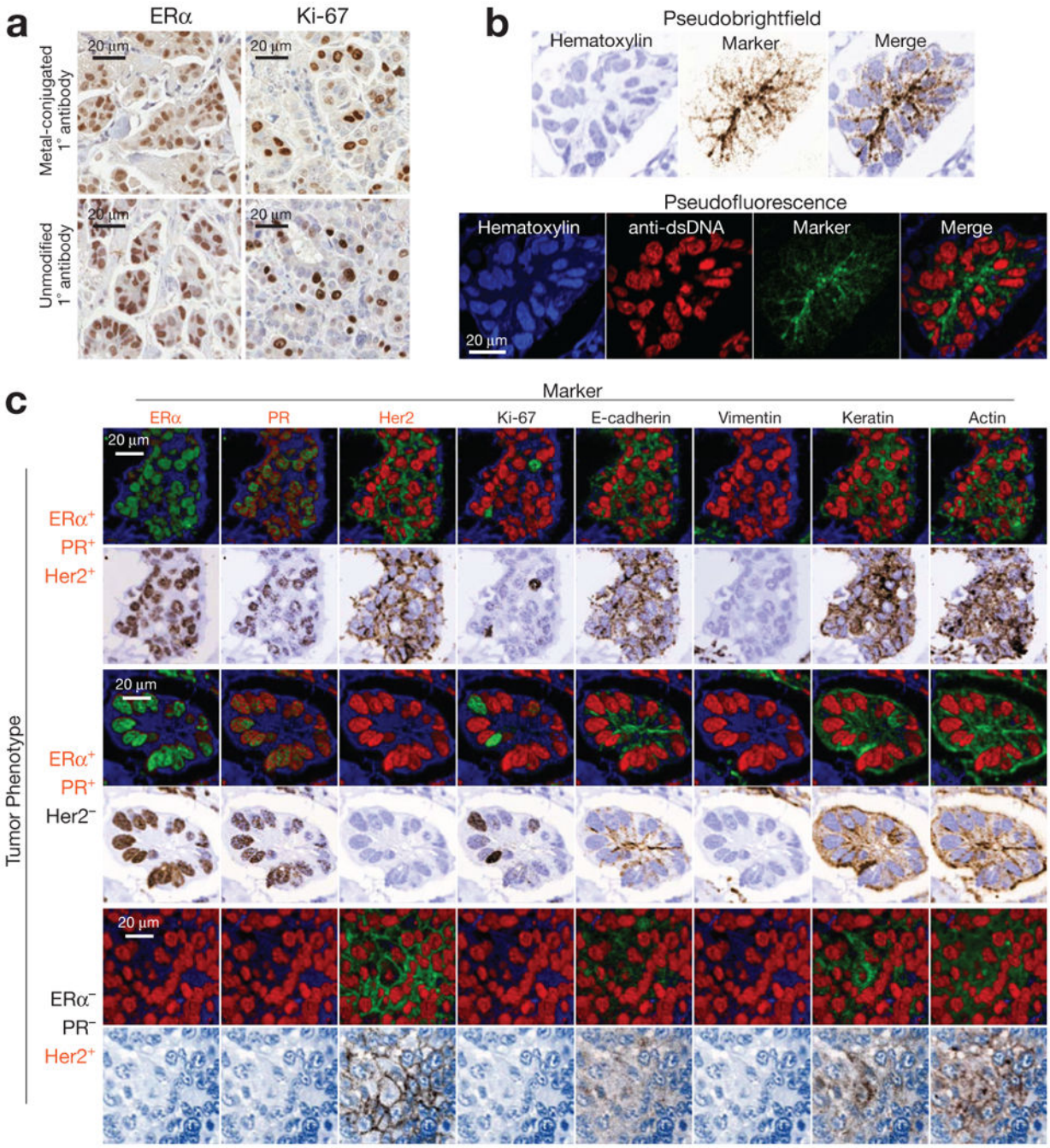

Figure 3. 10-color imaging of human breast tumors using MIBI

(**a**) Avidity of primary antibodies is unaffected by metal-conjugation. To access the effect of metal conjugation on antibody avidity, immunoperoxidase staining of serial sections from a single human breast tumor were stained with metal-conjugated or unmodified primary antibodies for Ki67 or ER-alpha. Positive-staining nuclei of comparable intensity were present in similar numbers when using metal-conjugated or unmodified primary antibodies. (**b**) Visual representation of MIBI data. Single channel ion data can be color mapped and merged to construct pseudo-brightfield or pseudo-darkfield images resembling conventional

immunoperoxidase or immunofluorescence staining, respectively. (**c**) 10-color imaging of human breast tumors. FFPE tissue sections from three different patients were analyzed using MIBI. HER2, ER, and PR are expressed appropriately with respect to the known immunophenotype of each specimen. ER, PR, and Ki67 demonstrate well-demarcated nuclear positivity, while e-cadherin, actin, HER2, and keratin expression is appropriately membranous. Field of view = 80 μm.

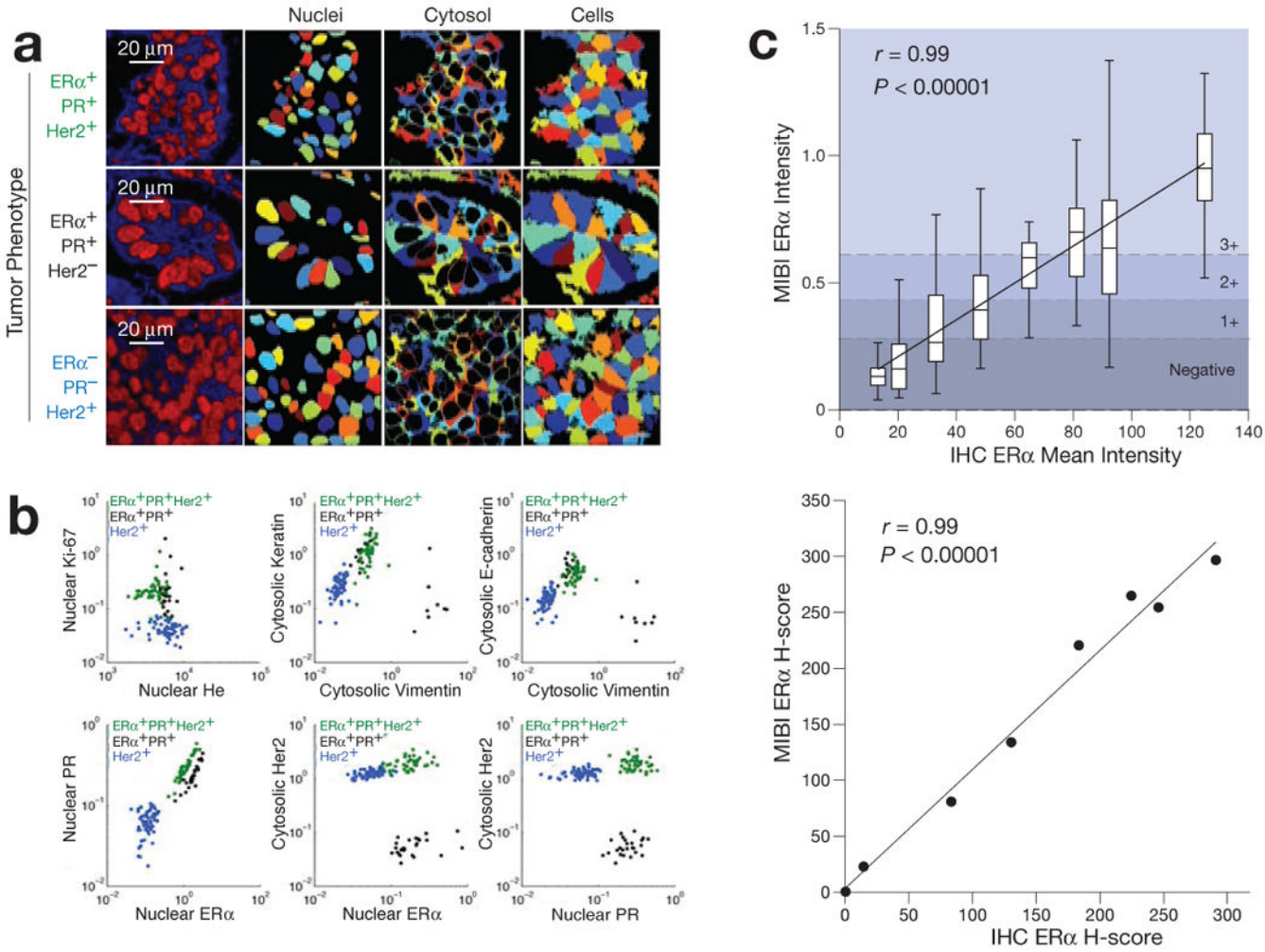

Figure 4. Quantitative analysis of tumor immunophenotype

(**a**) For quantitative single cell analysis, ion images are segmented into ROIs demarcating nuclear and cytoplasmic compartments. (**b**) Examination of the resultant data using conventional biaxial scatter plots demonstrates quantitative expression patterns matching the known immunophenotype of each respective tumor. Each point represents the mean pixel intensity for each respective cell ROI. Biaxial plots are log scaled. (**c**) Comparison of ER staining by IHC and MIBI. ER staining intensity of a cohort of breast tumors analyzed using IHC were compared with corresponding values attained using MIBI. Linear regression analysis comparing mean intensities (Top) and H-scores (Bottom) using the two methods demonstrates strong, robust agreement between the two methods ($r = 0.99$, $P < 0.0001$).

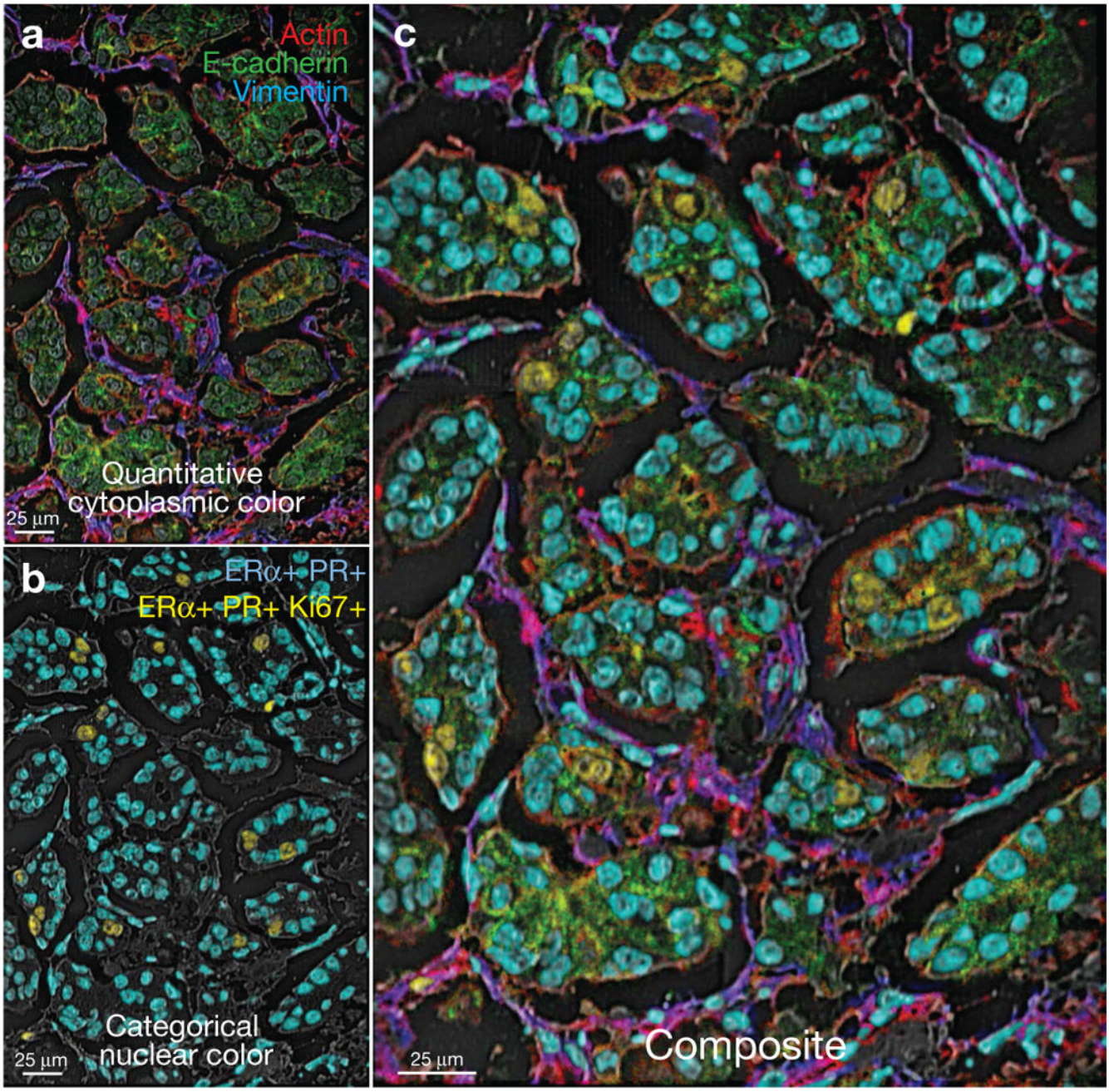

Figure 5. Composite representation of multidimensional MIBI data using categorical and quantitative colorization

(**a**) Quantitative colorization of cytoplasmic features. Green-encoded e-cadherin, red-encoded actin, and blue-encoded vimentin channels were merged to generate a quantitative representation of protein expression and colocalization. (**b**) Categorical colorization of nuclei. Subpopulations of $ER^+PR^+Ki67^+$ positive or ER^+PR^+ positive nuclei are pseudo-colored yellow or aqua, respectively. (**c**) Multidimensional data are summarized in a composite image illustrating quantitative and categorical expression patterns.